Marine Micropaleontology
January 2023, Volume 178, Pages 102187 (22p.)
https://doi.org/10.1016/j.marmicro.2022.102187
https://archimer.ifremer.fr/doc/00808/91997/

Pentaplacodinium lapazense sp. nov. from Central and Southern Gulf of California, a new non-toxic gonyaulacalean resembling *Protoceratium reticulatum*

Mertens Kenneth [1, *], Morquecho Lourdes [2], Carbonell-Moore Consuelo [3], Meyvisch Pjotr [4], Gu Haifeng [5], Bilien Gwenael [1], Duval Audrey [1], Derrien Amelie [1], Pospelova Vera [6], Śliwińska Kasia K. [7], Gárate-Lizárraga Ismael [8], Pérez-Cruz Beatriz [9]

[1] Ifremer, LITTORAL, F-29900 Concarneau, France
[2] Centro de Investigaciones Biológicas del Noroeste (CIBNOR), Av. IPN 195, Playa Palo de Santa Rita Sur, La Paz, Baja California Sur 23096, Mexico
[3] Oregon State University, Department of Botany and Plant Pathology, College of Agricultural Sciences, 2082 Cordley Hall, Corvallis, OR 97331-2902, USA
[4] Department of Geology, Ghent University, Krijgslaan 281, S8, 9000 Ghent, Belgium
[5] Department of Marine Biology and Ecology, Third Institute of Oceanography, Ministry of Natural Resources, Xiamen 361005, China
[6] Department of Earth and Environmental Sciences, University of Minnesota, 116 Church Street SE, Minneapolis, MN 55455, USA
[7] Department of Stratigraphy, Geological Survey of Denmark and Greenland, GEUS, Øster Voldgade 10, 1350 Copenhagen K, Denmark
[8] Instituto Politécnico Nacional, Centro Interdisciplinario de Ciencias Marinas, Av. IPN s/n, Playa Palo de Santa Rita, C.P. 23096 La Paz, Baja California Sur, Mexico
[9] Laboratorio Estatal de Salud Pública 'Dr. Galo Soberón y Parra', Boulevard Vicente Guerrero, Esq. Juan R. Escudero s/n, Ciudad Renacimiento, Acapulco, Guerrero, Mexico

* Corresponding author : Kenneth Mertens, email address : kenneth.mertens@ifremer.fr

lamorquecho@cibnor.mx ; carbonem@oregonstate.edu ; Pjotr.Meyvisch@UGent.be ; guhaifeng@tio.org.cn ; vpospe@umn.edu ; kksl@geus.dk ; igarate@ipn.mx

Abstract :

A new Pentaplacodinium species with six precingular plates is described from Bahía Concepción and Bahía de la Paz, Gulf of California. The non-fossil motile stage is described as Pentaplacodinium lapazense, whilst the fossil stage is described as Operculodinium lapazense. The cyst morphology is compared to topotype material of Operculodinium israelianum, which is larger, has longer processes and has a different wall structure. The motile cells display a plate formula of Po, Pt, X, 2′ + *2′, 6″, 6c, 7 s, 5‴, 1p, 1⁗. A typical gonyaulacalean fission line and plate overlap are observed. SSU-ITS-LSU ribosomal DNA sequences demonstrate that Pentaplacodinium saltonense is its closest relative. The species is homothallic. This species occurs in relatively shallow and restricted coastal areas, and has a preference for higher sea-surface temperatures and salinities. MicroFTIR spectra of the cysts are compared to spectra of cysts of other gonyaulacaleans and suggest very similar compositions. No yessotoxins were detected in any of the analyzed strains, hence, this species is unlikely to be responsible for the elevated

yessotoxin concentration observed in shellfish on the southern and central coastal region of the Gulf of California.

Highlights

► A new species *Pentaplacodinium lapazense* is described from the southwestern coastal region of the Gulf of California, Mexico. ► The plate formula is: Po, Pt, X, 2′+*2′, 6″, 6c, 7s, 5‴, 1p, 1⁗. ► The corresponding cyst stage is similar to *Operculodinium israelianum* and is named *Operculodinium lapazense*. ► No yessotoxins were detected in the analyzed ten strains.

Keywords : Operculodinium, Yessotoxins, Bahía Concepción, Bahía de La Paz, microFTIR spectroscopy

1. Introduction

Dinoflagellates are protozoans that can produce harmful algal blooms (HABs). These harmful species produce toxins which can accumulate in shellfish and other marine organisms. Many toxigenic dinoflagellates belong to the order Gonyaulacales and to either planktonic genera such as *Alexandrium, Lingulodinium,* and *Protoceratium*, or benthic such as *Gambierdiscus, Ostreopsis* and *Coolia* (e.g. Lassus et al., 2016, their table 1, p. 16). Yessotoxins (YTXs) is a family of toxins produced by the planktonic genera *Gonyaulax*, *Protoceratium* and *Lingulodinium* (e.g. Paz et al., 2008) and also potentially by *Pentaplacodinium* (Mertens et al., 2018). Yessotoxins are polycyclic ether-compounds that are considered to be potent cytotoxins; this caused the European authorities to establish a maximum permitted level in shellfish, which currently is 3.75 mg YTX equivalents/Kg (Regulation 786/EC/2013; Rubini et al., 2021). Yessotoxins have a high intraperitoneal toxicity, but their oral potency is very low (Tubaro et al., 2003); as such, YTX are not regulated by the CODEX standard, but are included in EU regulations.

Among the potential yessotoxin-producing genera listed above, *Pentaplacodinium* was most recently described (Mertens et al., 2018). It is closely related to the genera *Protoceratium* and *Ceratocorys* (Mertens et al., 2018) and with these genera, they form the Protoceratiaceae family (Luo et al., 2020). The type species, *Pentaplacodinium saltonense*, was originally described from the Salton Sea (California, USA) as having only five precingular plates. More recent morpho-molecular studies have shown that the genus

Pentaplacodinium encompasses a second species, *P. usupianum*, which bears six precingular plates (Luo et al., 2020).

Only cysts of *Pentaplacodinium saltonense* are known and have been related to the fossil-defined genus *Operculodinium*, although no formal taxon was erected for the fossil cysts of *P. saltonense*. *Operculodinium* currently includes 58 fossil-defined species (Williams et al., 2017), but only six of these species are considered to be extant (*O. aguinawense*, *O. crassum*, *O. giganteum*, *O. israelianum*, *O.*? *longispinigerum*, *O. psilatum*) in addition to the informal taxon *O. centrocarpum* sensu Wall and Dale 1966 (e.g. Limoges et al., 2020; Van Nieuwenhove et al., 2020). The International Code of Nomenclature for algae, fungi and plants (ICN, Turland et al., 2018), which governs the naming of dinoflagellate taxa, allows fossil- and non-fossil taxa to have separate names even when they are subsequently demonstrated to be linked.

Fourier transform infrared (FT-IR) spectroscopy is increasingly used on individual cysts by focusing and collecting the infrared (IR) beam with microscope objectives (micro-FT-IR) to investigate the geochemical composition of dinoflagellate cysts (e.g. Bogus et al., 2014; Meyvisch et al., 2021). The aim of such work is to develop chemotaxonomic tools, which will allow a better understanding of cyst taphonomy and the construction of paleoceanographical tools.

Bahía de La Paz and Bahía Concepción are embayments in the Gulf of California (Fig. 1). Mollusk fisheries from the Gulf of California form the majority of the total shellfish production of Mexico. Relatively high concentrations of yessotoxins have been recorded in Bahía de la Paz, although they did not exceed local regulatory levels (Leyva-Valencia et al., 2021), it highlights a need to study potential yessotoxin producing taxa. Of the 605 dinoflagellates that have been recorded from the Gulf of California (Hernández-Becerril 1987, Licea et al., 1995, Okolodkov and Gárate-Lizárraga, 2006), the most common and recurrent in

the region are the HAB species *Akashiwo sanguinea, Gymnodinium catenatum, Margalefidinium fulvescens*, and *M. polykrikoides* (e.g. Hernández-Becerril et al., 2007, Band-Schmidt et al., 2011, Gárate-Lizárraga et al., 2001, 2016), but regional yessotoxin producers are poorly known. Several dinoflagellate cyst studies have also been conducted on surface sediments from Gulf of California (e.g. Wall, 1986; Martínez-Hernández and Hernández-Campos, 1991; Morquecho and Lechuga-Devéze, 2003, 2004; Peña-Manjarrez et al., 2005; Pospelova et al., 2008; Limoges et al., 2010). Few of the yessotoxin producers have been studied in detail, except for *Lingulodinium* (Peña-Manjarrez et al., 2005), while some cysts related to *Gonyaulax* have been characterized morpho-molecularly (*Tectatodinium pellitum* and *Spiniferites mirabilis*; Gu et al., 2021). Dinoflagellate cysts have also been applied as paleoceanographical tools in the Gulf of California (e.g. Byrne et al., 1990; Price et al., 2013; Toscano-Cepeda and Helenes 2022)

Here we describe a new *Pentapharodinium* species, *P. lapazense* based on cells and cysts from Bahía Concepción and Bahía de La Paz, Mexico, and the corresponding fossil cyst as *Operculodinium lapazense.* The cyst morphology is compared to topotype material of *Operculodinium israelianum.* The macromolecular composition of the cyst wall is investigated using microFTIR spectroscopy. In addition, ten established strains were screened for yessotoxins.

2. Material and methods

2.1. Study area

Bahía Concepción (26° 39’ 39” N, 111° 48’ 58” W) is located on the central east coast of the Gulf of California (Figs 1A, B). It is approximately 45 km long by 10 km at the widest part. It

is a semi-enclosed and shallow bay, with a 30 m deep channel located in the northwestern portion and with a mixed semi-diurnal tidal regimen (Obeso-Nieblas et al., 1996). Hydrological conditions range from homogeneous and temperate in autumn and winter (16–20°C) to stratified and warm during spring and summer (28–32°C), (Morquecho and Lechuga-Devéze, 2004, Obeso-Nieblas et al., 2012). During the summer, in its internal and central basin, a strong thermocline isolates the bottom layer (20–30 m depth), which causes hypoxia and anoxia conditions to be generated in late summer and autumn (Lechuga-Devéze et al., 2000, López-Cortés et al., 2003, Morquecho and Lechuga-Devéze, 2004). Minimum temperature values were recorded from late fall through winter (16–20° C), and maximum temperature during summer (28–32° C) (Morquecho and Lechuga-Devéze, 2004). From May to October the prevailing winds are weak and primarily from the south. In late fall through early spring, the winds are strong and from the north (Thunell et al., 1994).

Isla San José (24° 58’ 23” N, 110° 36’ 52” W) is located in the northern end of Bahía de La Paz (Figs 1A, C). Its southwestern end is characterized by extensive beaches and a small lagoon of ~86 ha, which is bordered by a mangrove forest and a narrow sand bar (24° 52’ 32” N, 110° 33’ 30” W). Annual seawater temperature at Isla San José ranges from 17 to 30°C (Halfar et al., 2006).

Bahía de La Paz is the largest bay on the Baja California peninsular side of the Gulf of California (Figs 1A, C). The bay constantly exchanges water with the latter via a northern and a southern openings (e.g., Gómez-Valdés et al., 2003). Bahía de La Paz is subject to two main wind patterns, southerly and southeasterly winds, locally called Coromuel, prevailing from late spring to early autumn, with magnitudes of $4ms^{-1}$ combined with frequent calm periods. Strong and persistent northerly and northwesterly winds prevail in late autumn and winter, reaching velocities of 12 ms^{-1} (Muciño-Márquez et al., 2018).

2.2. Sample collection and treatment

Plankton and sediment samples were obtained from both the southwestern end of Isla San José and Bahía Concepción (Figs 1B, C). Four strains were established by isolating vegetative cells from Isla San José and two strains by hatching living cysts from Bahía Concepción using the micropipette technique according to Andersen and Kawachi (2005) by Lourdes Morquecho (Table 1). For the establishment and long-term maintenance of the strains, both f/2 (Guillard and Ryther, 1962) and GSe (Doblin et al., 1999) culture media were used. The f/2 medium was modified by adding H_2SeO_3 (10^{-8} M) and reducing the concentration of $CuSO_4$ to 10^{-8} M (Anderson et al., 1984). The seawater salinity used to prepare culture media varied between 37 and 39 psu. Established strains were grown at 20 ± 2 or 25 ± 2°C, with 40 µmol m^{-2} s^{-1} photon irradiance (12 : 12 h L : D), which are the standard conditions defined for the Marine Dinoflagellate Collection (CODIMAR, for its acronym in Spanish). Clonal or unialgal cultures are deposited in CODIMAR (Morquecho and Reyes-Salinas, 2004). A net phytoplankton sample was taken from Bahía de La Paz in August 2018 by Ismael Gárate-Lizárraga (sample C, 24°38'N, 110°01'W) and fixed with formaldehyde.

For hatching experiments, sediment samples from Isla San José were collected in 50 ml plastic tubes from the first centimeter of the sea floor by a scuba diver in 2014 (ISJ-A-1, 24°52' 28" N, 110°32'53' W). About 0.5 to 1.0 cm^3 of wet sediment was immersed in filtered seawater and, after one min of ultrasonication, the sediment was rinsed with filtered seawater through a 20 µm mesh metal sieve. From this residue, the cyst fraction was separated using the heavy-liquid sodium polytungstate (SPT) at a density of 1.3 g cm^{-1} (Bolch, 1997). Single cysts were then transferred to 0.5 mL microwells (Orange Scientific), subjected to an irradiance of 100 µmol photons m^{-2} s^{-1} and 24-h light, and filled with f/2 medium at room temperature and a salinity of 35 psu. Cysts were regularly checked for germination.

Observations were performed under a Leitz DM IL inverted light microscope. Encysted and excysted cysts, as well as motile cells, were photographed and measured using a Leica DM5000B light microscope with 100× oil immersion objectives.

For further morphological study of cysts and microFTIR spectroscopy, another sample from Isla San José was used (ISJ-B-4 2014, 24°52' 32.63" N, 110° 33'30.23" W). This sediment sample was rinsed through a 125 and 20 μm mesh metal sieve using filtered seawater and 10 % hydrochloric acid (HCl) to get rid of carbonates. All samples were stored in plastic bags in a refrigerator at 4 °C.

To compare the cyst morphology with *Operculodinium israelianum*, a sediment sample from the Reading 33/0 borehole (coord. 12944/16211, water depth 184 m) located in the Tel Aviv area (Issar, 1961; Moshkovitz, 1961; 1963, Reiss and Issar, 1961) at 167 m depth below seafloor on the Quaternary coastal plain of Israel was obtained through the Geological Survey of Israel (GSI). Palynological techniques were used for processing sediments (e.g., Mertens et al., 2012a). Material was rinsed twice with distilled water to remove salts. The samples were oven-dried at 40 °C and then treated with 10% HCl at room temperature to remove calcium carbonate particles. Samples were treated with 48–50% hydrofluoric acid (HF) at room temperature for two days to dissolve silicate particles, and then treated for 10 min at room-temperature HCl (10%) to remove fluorosilicates. The residue was rinsed twice with distilled water, ultra-sonicated for 30 s and finally collected on a 15 mm mesh. Aliquots of residue were mounted on microscope slides using glycerin jelly. To erect a cyst taxon for *Pentaplacodinium saltonense*, the slides were made using this same method (Mertens et al., 2018, p. 61).

2.3. Morphological study of thecate stages and cysts

For light microscopy, specimens were isolated using a micropipette, measured and photographed using an Olympus IX70 inverted light microscope equipped with differential interference optics and a digital camera DP72 (Olympus, Tokyo, Japan). For each thecate cell, the length was measured along the longitudinal axis, the width was measured along the middle of the cingulum, from one lateral margin to the other. All motile cell measurements in the species descriptions cite the minimum, average (in parentheses) and maximum values (in mm), in that order. The standard deviation (SD) is provided where appropriate. For each cyst, the lengths of the three longest visible processes with the corresponding widths at their base were measured within the focal plane. Process length was measured from the middle of the process base to the process tip. The average distance between processes was determined by measuring the distance between a process on the upper surface of the cyst near the center and the five processes nearest to it, as measured between the middle of the process bases as seen from the surface of the cyst. The central body wall thickness was measured at two to three positions around the cross section of each cyst. The central body maximum and minimum diameters were also measured unless specimens were overly compressed or broken. Fragments representing less than half of a cyst, and cysts with mostly broken processes, were not measured. All cyst measurements in the species description cite the minimum, average (in parentheses) and maximum values (in mm), in that order. The standard deviation (SD) is provided where appropriate.

For scanning electron microscopy (SEM), single specimens were isolated from the plankton samples using a micropipette on a IX70 (Olympus) inverted microscope. The cells were deposited on polycarbonate membrane filters (GTTP Isopore, 0.22 µm pore size; Millipore, Billerica, MA, USA), which were rinsed with distilled water. The filters were processed following the methods described in Couté (2002) and Chomérat and Couté (2008). They were dehydrated in a graded series of ethanol baths (15%–100%), critical point dried,

stuck to a stub using double-sided adhesive tape and coated with gold. The cells on the stubs were examined at the Station of Marine Biology in Concarneau using a Sigma 300 Gemini (Carl Zeiss Inc., Oberkochen, Germany) field-emission SEM equipped with both a conventional Everhart-Thornley and in-lens secondary electron detectors at 1.5 kV. Labelling of tabulation follows a modified Kofoidian system that recognizes homologs (Carbonell-Moore and Mertens 2019).

2.4. PCR amplifications and sequencing

Amplifications and sequencing at CIBNOR

Culture strains PEJV-6a, and PGCQ-1a (Table 1) were extracted from 25-mL cultures in logarithmic growth phase using the FastDNA® SPIN Kit for Soil (Catalog # 6560-200, MP Biomedicals, Solon OH, USA). For the PCR reaction, 1µl of DNA extract was used. For PCR, 25 pmol of each primer and 12.5 µL of PCR Master Mix 2X (Promega, Madison, WI, USA) containing the Taq DNA polymerase, dNTPs, $MgCl_2$ and reaction buffers were added in each tube. Three nuclear markers: small subunit (SSU) rDNA, large subunit (LSU) rDNA, internal transcribed spacer region (ITS1-5.8S rDNA-ITS2) were amplified using different cells. Several pairs of primers were used (Table 2). Two rounds of PCR were made. One µL of the dilution (1/100 in ddH_2O) of the PCR product was used as a DNA template for the second round of PCR. Almost the full length of the SSU rDNA (1,800 base pairs) was acquired. The PCRs for both rounds were performed using a TProfessional Basic thermocycler (Biometra GmbH, Goettingen, Germany) as follows: one initial denaturizing step at 94°C for 2 min, followed by 45 cycles each consisting of 94°C for 30 s, 56–62°C (depending on the primer pair used) for 30 s, 120 s (activation of the enzyme) and followed by 30 cycles of and 72°C for 4 min, and a final elongation of 72°C for 5 min. The PCR

products were purified using the Wizard SV Gel and PCR Clean-up system (Promega) according to manufacturer's recommendations. Results were confirmed on agarose gel (1%) after electrophoresis. For positive samples, PCR products were purified with the ExoSAP-IT PCR Product Cleanup Reagent (Affymetrix Inc., Cleveland, Ohio, USA). The sequencing reaction was carried out using the ABI PRISM BigDye Terminator Cycle Sequencing Kit (Applied Biosystems, Carlsbad, CA, USA), and the sequences were determined using an automated 3130 genetic analyzer (Applied Biosystems).

*Amplifications and sequencing at Ifremer*A single cell hatched from a cyst (PAZA2) was isolated from surface sediment from Isla San José (Table 1) for single-cell PCR using a micropipette. The identification and photography were carried out using an Olympus IX70 inverted light microscope equipped with differential interference optics and a digital camera DP72 (Olympus, Tokyo, Japan). Each cell was individually rinsed in several drops of double distilled water (ddH_2O) and immediately transferred to a 0.2 mL PCR tube containing 5 µL of ddH_2O. PCR tubes were stored at -20°C. For PCR, the samples were thawed, and 25 pmol of each primer and 12.5 µL of PCR Master Mix 2X (Promega, Madison, WI, USA) containing the Taq DNA polymerase, dNTPs, MgCl2 and reaction buffers were added in each tube. Two rounds of PCR were realized and 1 µL of the dilution (1/100 in ddH2O) of the PCR product was used as a DNA template for the second round of PCR. Almost the full length of the SSU rDNA (1,800 base pairs) was acquired. The PCRs for both rounds were performed using a TProfessional Basic thermocycler (Biometra GmbH, Goettingen, Germany) as follows: one initial denaturizing step at 94°C for 2 min, followed by 30 cycles each consisting of 94°C for 30 s, 56-62°C (depending the primers used) for 30 s, and 72°C for 4 min, and a final elongation of 72°C for 5 min. Culture strains PEJV-2a, PEJV-3b, and PEJV-4a were extracted with PCRBIO Rapid Extract PCR Kit (PCR Biosystems Ltd) which combines extraction and

PCR. In a 1.5 mL tube, 1ml of culture were taken and centrifuged for 3 minutes at 14,000 rpm. The supernatant was discarded to retain only the pellet. Then the manufacturer's instructions were followed, except for the step dilution where 190 µL of PCR grade dH_2O were added instead of 900 µL. The pair of primers used for the PCR is ITSFW and D3B (Table 2) with a Tm of 60°C. PCR-amplified product was visualized on an agarose gel after electrophoresis and the positive samples were purified using the ExoSAP-IT PCR Product Cleanup reagent (Affymetrix, Cleveland, OH, USA). A Big Dye Terminator v3.1 Cycle Sequencing Kit (Applied Biosystems, Tokyo, Japan) was used for sequencing of the amplicon generated. Primers and excess dye-labeled nucleotides were first removed using the Big Dye X-terminator purification kit (Applied Biosystems, Foster City, CA, USA). Sequencing products were run on an ABI PRISM 3130 Genetic Analyzer (Applied Biosystems).

2.5. Sequence alignments and phylogenetic analysis

Newly obtained SSU, LSU rDNA and ITS region sequences were incorporated into closely related sequences downloaded from the GenBank nucleotide database (NCBI). The nucleotide sequences were aligned using MAFFT v7.110 (Katoh and Standley, 2013, http://mafft.cbrc.jp/alignment/server/) with the default settings.

The most appropriate models were chosen by jModelTest (Posada, 2008) with Akaike Information Criterion. Bayesian inference (BI) was performed on the data matrix using MrBayes 3.2 (Ronquist and Huelsenbeck, 2003) and the best model (GTR+G). Four Markov chain Monte Carlo (MCMC) chains were performed for 2,000,000 generations, sampling every 1000 generations. The first 10% of burn–in trees were discarded. A majority rule consensus tree was reconstructed to examine the posterior probabilities of each clade. Maximum likelihood (ML) was performed using RaxML v.7.2.6 (Stamatakis, 2006) on the T–

REX web server (Boc et al., 2012). Node support was assessed with 1000 bootstrap replications.

2.6. Extraction and analysis of yessotoxins

For the established strains (Table 1), a cell pellet was collected by centrifugation in microtubes at late exponential phase of growth (about 10^3 – 10^4 cells), and stored at -20 °C. For the extraction, 400 µL of methanol were added to the cell pellet and the mixture was transferred in a 1.5 mL Safelock Eppendorf tube. Glass beads (100–250 µm in diameter) were added before cell lysis using a Mixer Mill equipment (MM400, Retsch) at 30 Hz for 30 min. After centrifugation at 15,000 g, the supernatant was transferred into a 1.5 mL Eppendorf tube. The cell pellet was re-extracted with 400 µL of methanol and shaking at 30 Hz for 30 minutes. After centrifugation at 15,000 g, the supernatants were pooled and evaporated to dryness with a gentle stream of nitrogen at a temperature of 30°C. The residue was dissolved in 300 µL of methanol. The extract was ultrafiltered (0.20 µm, Nanosep MF, Pall) and transferred into an HPLC vial before LC–MS/MS analyses.

Sample analyses were performed to detect 13 yessotoxin analogues by LC-MS/MS using a Shimadzu UFLCxr system coupled to a triple quadruple hybrid mass spectrometer Q-Trap (API400QTrap, Sciex) equipped with a heated electrospray ionization (ESI) source as detailed in Wang et al., (2019).

2.7. FTIR spectroscopy

Multiple specimens of different gonyaulacalean dinoflagellate cyst species, including *Operculodinium lapazense*, were retrieved from sediment samples and residues for FTIR

spectroscopy (Table 3). Droplets of these processed samples were examined under a Zeiss Primovert inverted microscope (400X magnification) from which visually clean dinocysts were manually picked using a hand-crafted glass Pasteur pipette with an attached rubber suction tube. Individual specimens were iteratively cleaned by transferring them to several droplets of distilled water, while rinsing the Pasteur pipette with distilled water in between each transfer. Afterwards, for each specimen multiple z-slice images were taken with a Zeiss AxioCam MRc 5 at 400× magnification.

Prior to FTIR measurement, individual specimens were transferred to a Mid-Infrared Enhanced Gold Mirror (Thorlabs®) and care was taken to leave no visual, surrounding drying spot. Afterwards, deposited specimens were analyzed with a Bruker Hyperion 2000 IR microscope coupled to a Bruker Vertex 80v FTIR spectrometer, located at the Department of Solid State Sciences (Ghent University). The spectra were collected in ATR (attenuated total reflection) micro-FTIR mode, using a germanium crystal with a tip diameter of 100 µm, which was brought into direct contact with the samples. For each specimen, an infrared spectral range of 4500–600 cm^{-1} at a 4 cm^{-1} resolution and averaged over 256 scans was recorded using a liquid N_2-cooled MCT detector and KBr beamsplitter in the microscope and a Globar IR source in the spectrometer unit. Subsequent spectral data preprocessing was done in OPUS 8.2.21 (Bruker®) and included (in the following order): atmospheric compensation (removal of residual atmospheric CO_2 and H_2O absorption bands in the spectra), Savitzky-Golay smoothing (polynomial order of 2 and a window size of 13) and baseline correction (rubberband correction using polynomes and 128 baseline points, one iteration). For each of the species from a given sample (Table 3) an average spectra was calculated, which were visualized and min-max normalized over the range of 4000–600 cm^{-1} to make them more intercomparable and which were used for qualitative profiling. Absorption bands were

assigned via Coates (2000), Versteegh et al. (2020), Mertens et al. (2021), and Meyvisch et al. (2021).

3. Results

3.1. Study of plankton samples, culture strains, germination experiments, and surface sediments

Investigation of plankton and sediment samples from Bahía Concepción, Isla San José, and Bahía de La Paz revealed the presence of a species that is superficially similar to *Protoceratium reticulatum* and to *Pentaplacodinium satanense*. This species is here assigned to *Pentaplacodinium lapazense* sp. nov. Cultures were established from both plankton samples, and germination of living cysts (Table 1). Another process-bearing cyst was isolated from a surface sediment sample of Isla San José (Table 1) and identical thecate stages emerged from these cysts (Fig. 2). The cells were morphologically identical to specimens observed in plankton samples (Fig. 2), as well as to specimens from several culture strains (Figs. 2–3), as described below. A small number of resting cysts were formed in monoclonal strain PEJV-3 (established from a vegetative cell), suggesting that the species is homothallic. *Pentaplacodinium lapazense* from Isla San José was found at seawater temperature and salinity ranges between 29.5–30.3°C, and 36.1–36.4 psu respectively, and shared its habitat with other dinoflagellates belonging to the genera *Coolia*, *Margalefidinium*, *Prorocentrum*, and *Pyrophacus*.

3.2. Systematics

Division DINOFLAGELLATA (Bütschli, 1885) Fensome et al., 1993

Class DINOPHYCEAE Pascher 1914

Subclass PERIDINIPHYCIDAE Fensome et al., 1993

Order GONYAULACALES Taylor 1980

Suborder Gonyaulacineae autonym

Family Protoceratiaceae Lindemann 1928 emend. H.Gu et Mertens in Luo et al., 2020

Genus *Pentaplacodinium* Mertens, Carbonell-Moore, Pospelova et Head emend. H.Gu et Mertens 2020

Pentaplacodinium lapazense Mertens, Carbonell-Moore, Gárate-Lizárraga, Morquecho sp. nov. (Figs. 2–6)

Synonymy:

2009 "*Protoceratium globosum*" Kofoid et Michener; Morquecho et al., p. 18, 20, figs. 13–17.

2016 "*Protoceratium reticulatum*" (Claparède et Lachmann) Bütschli and "*Protoceratium globosum*" Kofoid et Michener; Morquecho-Escamilla et al., 2016, plate 7, figs. 1–9, plate 8, figs. 1–9.

Diagnosis: Theca roundish. The theca has an L-type ventral organization and dextral torsion. The plates may be lightly to heavily reticulated or with multiple depressions. Inside each reticulation or depression, a pore may be found. The ends of the descending cingulum are displaced by ~1.0 widths. Plate formula Po, Pt, X, 2′+*2′, 6″, 6c, 7s, 5‴, 1p, 1⁗.

Etymology: The specific epithet refers to the type locality for this species.

Type locality: Bahía de La Paz (at 24° 52'31.82"N, 110° 33'27.28"W), Baja California Sur, Mexico.

Gene sequence: The 28S, ITS and 18S rDNA gene sequence of the culture PEJV-3, established from plankton from Isla San José northern border of Bahía de La Paz (Table 1). — GenBank Accession No. OP806525–OP806525 (18S), OP806527–OP806527 (ITS), and OP806529–OP806534 (28S). All other strains are considered to belong to the same species (Table 1).

Holotype: The SEM stub 19G01 containing the type (specimen shown in Fig. 3A) has been deposited at the dinoflagellate type collection in the Centre of Excellence for Dinophyte Taxonomy (CEDiT, Wilhelmshaven, Germany), which is part of the Herbarium Senckenbergianum Frankfurt/M. (FR) with the designation CEDiT2022H138.

Description: Motile cells observed in Bahía de La Paz plankton samples and the established cultures (Figs. 2–8). Thecae have a roundish shape (Figs 2D–E) and a typical sexiform gonyaulacoid hypothecal tabulation (sensu Fensome et al., 1993b, text-fig. 64B) with an L-type ventral organization (sensu Fensome et al., 1993b, text-figs. 82A, C) and dextral torsion (sensu Fensome et al., 1993b, text-fig. 83C). The epitheca is shorter in length than the hypotheca. The plates may be lightly to heavily reticulated or present multiple depressions. Inside each reticulation or depression, a pore may be found. All pores each contain several minute pores (Fig. 3B). The reticulations are faintly expressed on the sulcus and cingulum (Fig. 3E). The cell content is brown-yellowish due to the presence of chloroplasts (Figs. 2D-E). No red bodies are present. The nucleus lies in the hypotheca (Fig. 2E).

The apical pore complex (APC) consists of an elongated cover plate (Pt) surrounded by a pore plate (P_o). There is a small X plate between the left end of Po and the anterior end of plate 1′ (Figs. 4C–G). The cover plate widens ventrally, it is often missing (e.g., Fig. 4F). The pore plate may have from five to seven large pores. A low collar largely surrounds the pore plate and is formed by the raised edges of the first and second apical plates, as well as the fourth apical homolog plate (Fig. 3A). The first apical plate (1′) is rectangular, whereas the

second apical plate (2′) and the fourth apical homolog plate (*4′) are six-sided and seven-sided respectively and irregularly shaped (Fig. 3A). The third apical homolog plate (*3′) is small, pentagonal and contacts plates 2′ and *4′, and in the specimens observed it never contacted the pore plate (Fig. 3A). There is a large round ventral pore located posteriorly between plates 1′ and *4′ (Fig. 3A, E). The precingular series consists of six large plates, where 2″ is the largest, and 6″ is the smallest. If the contact with the cingular plates is counted as a single suture (irrespective whether one or two cingular plates are present), then plates 1″, 3″, and *5″ are five-sided, 2″ is four-sided, while *6″ is six-sided (Fig. 3A). There is hardly any contact between the anterior sulcal plate and 1′ (e.g., Fig. 3E). The contact of 1′ with both the pore and X plates and 2′ results in an insert configuration (sensu Fensome et al., 1993, text-fig. 62A). The cingulum is left-handed (descending), vested with narrow lists, and composed of six cingular plates. The ends of the cingulum do not overhang and are displaced by ~1.0 widths (Fig. 3E).

The sulcus narrows anteriorly and consists of seven plates (Figs. 5, 6). The first postcingular plate 1‴ is treated here as a sulcal and labeled the anterior left sulcal plate (Ssa) (Carbonell-Moore et al., 2022). The hook-shaped anterior sulcal plate (Sa) is relatively large and lays between plates 1″ and *6″, barely contacting plate 1′ (Fig. 3E, Figs. 5, 6). Between the Sa plate and the Sda (right anterior sulcal plate), the small anterior right accessory sulcal plate (Sdaa) lays. The anterior left sulcal plate (Ssa) is somewhat smaller than the anterior right sulcal plate (Sda). Below the Sda lays the small posterior right sulcal (Sdp) and below the Ssa a much larger plate, the left posterior sulcal (Ssp). The flagellar pore (FP) is surrounded by Sa, Sdaa, Sda, Ssa, Sdp and Ssp. Lists of Sda and Ssa can partly cover the FP. Lastly, below the Sdp and Ssp there is the large posterior sulcal plate (Sp), whose sutures with the adjacent non-sulcal plates are lined with pores and depressions (Fig. 3E, Fig. 5).

The hypotheca is asymmetrical as a consequence of dextral torsion (Fig. 3C). There are five postcingular homolog plates. Plate *2‴ is the smallest in the series. All other postcingular plates are large, they are trapezoidal (Fig. 3C). The posterior intercalary plate (1p) does not bear a flange on its right margin (Fig. 3E). The large antapical plate 1‴″ was sometimes split into two plates in the cultures (Fig. 3D).

The fission line was observed in cultures, it was located along 3″, 4″, 5″, 6″, 1p, 1‴″, 5‴ and 3″, 2′, *3′, *4′, 1′, Ssa, *2‴, *3‴, *4‴ (Figs. 7, 8).

The plate overlap pattern (Fig. 8A, C) shows plate 3″ forming the keystone plate (the plate that overlaps all adjacent plates) in the epitheca, while plate *4‴ forms the keystone plate in the hypotheca. The plate overlap is identical to the one reported for *Pentaplacodinium saltonense* by Mertens et al., 2018, fig. 4A.

Dimensions: Cultured cells established from Bahía Concepción and Isla San José: length, 28.2 (41.4) 56.4 µm (SD=7.3, n=195); width, 28.2 (39.8) 56.4 µm (SD= 6.9, n=211).

Comments: Pentaplacodinium lapazense sp. nov. is defined from the characters of the motile stage, these distinguishing it from its congeners (Table 4). *P. lapazense* differs from *P. saltonense* in the number of precingular plates (six vs. five), in that the posterior intercalary plate (1p) does not bear a conspicuous flange on its right margin, and in that the ends of the cingulum are displaced by only ~1.0 widths vs. 2.0 widths. *P. lapazense* differs from *P. usupianum* in the absence of a ventral pore in the latter, a smaller size of the latter (26.6–31.3 µm long and 22.7–27.7 µm wide) and the presence of spines at the antapical end also in the latter (Luo et al., 2020). It is more similar to *Protoceratium reticulatum* which is more polyhedral and bears a sigmoidal cover plate, as opposed to a roundish and elongated cover plate that widens ventrally in *P. lapazense*. It differs from the obscure species *Protoceratium globosum* Kofoid et Michener in that the latter has no pores (Kofoid and Michener 1911, p. 278, no illustration).

Remarks. The cyst corresponds to the fossil-based taxon *Operculodinium lapazense*, which is described below.

Operculodinium lapazense Mertens, Morquecho, Carbonell-Moore, Gárate-Lizárraga, sp. nov. (Figs. 9, 10a–f)

Synonymy:

"*Operculodinium israelianum*" (Rossignol) Wall; Wall 1967, p. 111, plate 16, figs. 3–4; non Rossignol 1962, 1964.

? "*Operculodinium israelianum*" (Rossignol) Wall; Wall 1968, p. 181, plate 3, figs. 2–3.

? "*Operculodinium israelianum*" (Rossignol) Wall; Martínez-Hernández and Hernández-Campos 1991, p. 37, plate 2, fig. 3.

? "*Operculodinium centrocarpum*" (Deflandre and Cookson) Wall; Peña-Manjarrez et al., 2005, plate 3, Fig. 6.

Diagnosis: The cysts have an approximately spherical central body with a thin pedium and thicker spongy-fibrous luxuria that are not very densely packed. Process distribution apparently intratabular. Processes fibrous and distally tapering, and have acuminate to minutely expanded distal ends. The archeopyle corresponds to the 3″ precingular plate and has a smooth margin with rounded angles. The operculum is free. A flagellar scar is present.

Holotype. The SEM stub 21K03 containing the holotype (specimen shown in Fig. 9b) is deposited at the dinoflagellate type collection in the Centre of Excellence for Dinophyte Taxonomy (CEDiT, Wilhelmshaven, Germany), which is part of the Herbarium Senckenbergianum Frankfurt/M. (FR) with the designation CEDiT2022H140.

Type locality. Surface sediment from Isla San José northern border of Bahía de La Paz (ISJ-B-1 2014, 24°52' 32.63" N, 110° 33'30.23' W, 7m water depth).

Collection date. 13/04/2014.

Habitat. Marine.

Etymology. The specific epithet refers to the type locality for this species, Bahía de La Paz.

Description. Cysts from Isla San José northern border of Bahía de La Paz surface sediments (Figs. 9–10). The central body is approximately spherical. The wall is thick, consisting of a thin, solid pedium that has a smooth inner surface, and a thicker spongy-fibrous luxuria that that are not very densely packed. Processes are numerous and are solid and fibrous along their entire length, often loosely fibrous at the base. Process bases are expanded, and larger processes may be concave in lateral profile for at least half of their length. Some closely adjacent processes are joined at the base. Most processes usually have a minute distal expansion, observed under SEM as a concave platform ~1.0 µm or less in diameter with strongly irregular margins that may be approximately perpendicular to the shaft. Alongside these, some processes on most specimens taper to distal points, and such processes occasionally predominate on individual specimens. Processes are mostly of even height, but shorter and thinner processes may be interspersed. Processes are not evenly spaced, and their parallel alignment and bands devoid of processes observed in many specimens suggest intratabular distribution. There is however no clear evidence of tabulation except for the archeopyle and often parallel alignment along the cingular margins. The archeopyle is moderately wide and reflects the precingular thecal plate *3", whereas the operculum is released as a single piece. A flagellar scar is present (Fig. 9F).

Dimensions. Cysts from surface sediments of Isla San José: maximum central body diameter, 43.3 (50.6) 63.8 µm (SD=6.6, n=13); minimum central body diameter, 42.5 (48.1) 57.8 µm (SD=5.0, n=13); average length of three processes per cyst, 3.4 (5.4) 7.4 µm (SD=1.1, n=39) and wall thickness 0.4 (1.4) 3.2 (SD=0.6, n=30). This overlaps with ranges provided by Wall (1967): 40–65 µm (body diameter) and 3–6 µm (process length).

Remarks. The geological preservability of these cysts was demonstrated by their ability to withstand palynological treatment. The observed cysts correspond most closely to the fossil based species *Operculodinium israelianum* (Rossignol 1962) Wall 1967 described from the Pleistocene of Israel, and *Operculodinium psilatum* Wall 1967 described from the postglacial (Holocene) of the Caribbean. However, *Operculodinium israelianum* has averagely longer processes (Fig. 11), no flagellar scar and has more densely packed fibrils (see below), and *O. psilatum* has a psilate surface interrupted by minute and sparsely distributed processes, and a pronounced cingulum (Wall, 1967). Both have archeopyles that are less wide than for the cyst of *P. saltonense*. *Operculodinium saltonense* has averagely shorter processes, can have a composite archeopyle and does not have a flagellar scar.

Operculodinium israelianum (Rossignol 1962) Wall 1967, p. 111 emend. nov. Mertens and Pospelova (Fig. 12)

Synonymy.

'Hystrichosphaeridium israelianum' Rossignol 1962, p. 132, plate 2, fig. 3 [Not validly published].

'Baltisphaeridium israelianum' (Rossignol 1962) Downie and Sarjeant 1965, p. 91 [Combination not validly published].

'Cleistosphaeridium israelianum' (Rossignol 1962) Davey et al., 1966, p. 170 [Combination not validly published].

'Cordosphaeridium israelianum' (Rossignol 1962) Lentin and Williams 1993, p. 126 [Combination not validly published].

Cleistosphaeridium cephalum Kar 1985

?Hystrichosphaeridium westii Deflandre in West 1961, p. 465 [Not validly published: no description or illustration]

Diagnosis. The cysts have an approximately spherical central body with a thin pedium and thicker spongy-fibrous luxuria that has densely packed fibrils. Process distribution apparently intratabular. Processes fibrous and distally tapering, and have acuminate to minutely expanded distal ends. The archeopyle corresponds to the 3" precingular plate and has a smooth margin with rounded angles. The operculum is free. No flagellar scar is present.

Dimensions. Cysts from Reading 33/0 borehole (coord. 12944/16911, water depth 184 m) at 167 m depth below seafloor: maximum central body diameter, 45.2 (56.4) 70.2 µm (SD=6.5, n=43); minimum central body diameter, 41.4 (52.1) 66.4 µm (SD=7.1, n=25); average length of three processes per cyst, 6.4 (10.5) 15.3 µm (SD=2.3, n=147) and wall thickness 0.2 (1.2) 2.5 (SD=0.5, n=147). This overlaps with ranges provided by Rossignol: 45–65 µm (body diameter) and 6–10 µm (process length).

Holotype. Rossignol 1962, p. 132, plate 2, fig. 3.

Type locality. Pleistocene of the Ashdod 15/0 borehole, Israelian coastal plain [It is somewhat difficult to assess what the precise age is of the holotype of *Operculodinium israelianum*. Rossignol (1962) did not specify the locality of the holotype, but since the interval between 80 and 190 m depth below seafloor of the Ashdod 15/0 borehole was primarily studied in this publication, it can be assumed that it must be Pleistocene in age. Our material from the Reading 33/0 borehole at 167 m depth, is here thus assumed to be topotype material.]

Collection date. Not known.

Habitat. Marine.

Remarks. The difference between *Operculodinium israelianum* and *Operculodinium centrocarpum sensu stricto* requires further study as both taxa seem to intergrade (Head, 1996). For comparison with *O. saltonense* and *O. lapazense,* see above.

Operculodinium saltonense K.N. Mertens, M.C. Carbonell-Moore et V. Pospelova sp. nov. (Fig. 13)

Diagnosis: The cysts have an approximately spherical central body with a thin pedium and thicker spongy-fibrous luxuria. Process distribution apparently intratabular. Processes fibrous and distally tapering, have acuminate to minutely expanded distal ends. The archeopyle corresponds to the *(3" + 4") precingular plate and has a smooth margin with rounded angles. The operculum is free. No flagellar scar is present.

Dimensions. Palynologically treated cysts from surface sediments of the Salton Sea: maximum central body diameter, 48.6 (56.3) 70.9 µm (SD = 5.3, n = 23); minimum central body diameter, 45.7 (52.1) 61.4 µm (SD = 3.8, n = 22); average length of three processes per cyst, 1.0 (3.1) 5.7 µm (SD = 1.2, n = 66); process width at base 1.0 (2.2) 3.9 µm (SD = 0.6, n = 66) and wall thickness 0.9 (1.6) 2.4 µm (SD = 0.4, n = 66).

Holotype. Specimen on microscope slide 1 of station 5 (UVic2013-271). The microscope slide containing the type (specimen shown in Figs. 13a–c) is deposited at the dinoflagellate type collection in the Centre of Excellence for Dinophyte Taxonomy (CEDiT, Wilhelmshaven, Germany), which is part of the Herbarium Senckenbergianum Frankfurt/M. (FR) with the designation CEDiT2022H139.

Type locality. The Salton Sea, California, USA (station 5 at 33,50°N, -115,91°E, 0.2 m water depth).

Collection date. 24 October 2013.

Habitat. Marine.

Remarks. Mertens et al., (2018) did not erect a fossil-defined name for the cyst of *P. saltonense*; this is achieved here by selecting a fossil holotype. For comparison with *O. israelianum* and *O. lapazense,* see above.

3.3. Phylogenetic position of P. lapazense *and other studied strains*

The LSU rDNA based phylogenetic tree demonstrates that all sequences of *P. lapazense* are identical and form a sister-clade to *P. saltonense* and *P. usupianum* with significant support (100/0.86; Fig. 14). *P. reticulatum* and *P.* cf. *reticulatum* and several *Ceratocorys* species form two separate clades within the same larger clade (Protoceratiaceae), with significant support (Fig. 14). The LSU rDNA sequences do not allow separation of the *Ceratocorys* species. The SSU rDNA based tree yielded very similar results as the LSU rDNA based tree, with significant support for the same clades (Fig. 15). The ITS based tree again showed significant support for the same clades, but longer branches separate the species (Fig. 16).

3.4. Yessotoxin analysis

None of the ten examined strains of *Peridiniplacodinium lapazense* produced detectable yessotoxins (Table 5). Limits of detection for YTX ranged between 0.18 and 0.57 fg cell^{-1} depending on cell numbers in each pellet.

3.5. microFTIR spectroscopy

Average ATR micro-FTIR spectra of the analyzed dinoflagellate cyst species (Fig. 17) show two wavenumber regions with assignable absorption bands (Table 6): 3600–2800 cm^{-1} and 1750–600 cm^{-1} (fingerprint region). The relative intensities of absorption peaks were calculated to compare the average spectra (Table 7).

4. Discussion

4.1. Morphological observations of the thecate stage and culture observations

The discovery of a new *Pentaplacodinium* species with six precingular plates, confirms previous observations that the genus *Pentaplacodinium* can have five or six precingular plates (e.g., Luo et al., 2020). The close similarity of the morphology of the thecate stage of *P. lapazense* to *Protoceratium reticulatum*, suggests that care should be taken to correctly identify these species. The apical pore complex clearly is important to differentiate such genera.

The fission line observed in *P. lapazense* follows the boundaries between the respective epithecal plates 3", 4", 5", 6", Sa and 2", 2', *3', *4', 1', 1" and the respective hypothecal plates Ssa, 1p, 1"", *5"' and *2"', *3"', *4"'. A fission line along those boundaries is typical for gonyaulacaleans such as *Gambierdiscus* (Loeblich III and Indelicato 1986), *Gonyaulax* (Dodge 1988), *Alexandrium* (Tillmann et al., 2020) and *Lingulodinium* (Tillmann et al., 2021). The plate overlap is typical for gonyaulacaleans, with 3" forming the keystone plate (the plate that overlaps all adjacent plates) on the epitheca, and *4" forming the keystone plate on the hypotheca (Fig. 3B, D).

The discovery of an *X* plate in *Pentaplacodinium lapazense* contributes to the growing evidence of the existence of such a small plate in gonyaulacaleans such as *Acanthogonyaulax* (Carbonell-Moore and Mertens, 2020) and *Lingulodinium* (Tillmann et al., 2021). As remarked by Tillmann et al. (2021), such an X Plate can also be seen in *P. saltonense* (Mertens et al., 2018, fig. 7F).

The formation of resting cysts in monoclonal strains suggests that this species homothallic, just like *Protoceratium reticulatum* (Salgado et al., 2017).

4.2. Morphological observations of the cyst stage

Although *Operculodinium lapazense* is fairly similar to *O. saltonense* and *O. israelianum*, it may be differentiated using the packing of fibrils in the wall structure, process length and the presence or absence of a flagellar scar (Table 8). However, process length has been considered to vary infraspecifically, specifically for the species *Lingulodinium* (e.g. Mertens et al., 2009) and *Pyrodinium* (Mertens et al., 2015). In contrast, in *Protoceratium*, which has also been related to fossil *Operculodinium*, there is intraspecific variation that is related to process length variation (Mertens et al., 2012b; Jansson et al., 2014; Wang et al., 2019). For *Pentaplacodinium*, where two species are now related to the fossil genus *Operculodinium*, there is evidence that the process length variation between both taxa is related to intraspecific variation. This has important implications for fossil taxa, where morphological variations of process length have been considered intraspecific, as exemplified by *Pentaplacodinium*.

4.3. Phylogenetics

All phylogenetic trees support that *P. lapazense* is a closely related but is a separate species from the other two *Pentaplacodinium* species (Figs. 13–15). There is also strong support for *Ceratocorys, Protoceratium, Pentaplacodinium* to belong in one family, the Protoceratiaceae. This is in line with previous observations (Wang et al., 2019; Luo et al., 2020).

4.4. Biogeography and ecology of Pentaplacodinium lapazense

According to plankton and cyst observations, *P. lapazense* could be found in restricted and shallow waters of tropical to subtropical regions. This new species seems to have a preference

for higher seawater temperatures and salinities. In Bahía Concepción, seasonal abundance of meroplankton dinoflagellates and relationships with yields of newly-formed cysts coincide with hydrographic transitional periods in the water column in spring (20–24°C) and early fall (24–28°C) (Morquecho and Lechuga-Devéze, 2004). In Bahía Concepción (Verdugo-Díaz, 1997), Bahía de La Paz (Obeso-Nieblas et al., 2008), and Isla San José the annual salinity range oscillates between 34.5–37 psu. The site in Isla San José from where most of the strains were isolated, is a small and shallow mangrove lagoon where dinoflagellates are more frequent during summer. *Pentaplacodinium lapazense* was found at seawater temperature and salinity ranges between 29.5–30.3°C, and 36.1–36.4 psu respectively, and sharing habitat with other dinoflagellates of the genera *Coolia*, *Margalefidinium*, *Prorocentrum*, and *Pyrophacus*.

4.5. Yessotoxin production

This study demonstrated that *P. lapazense* strains from Mexico do not produce any yessotoxins within detection limits. Previous studies demonstrated that *P. usupianum* did not produce either detectable amounts of toxins (Luo et al., 2020). Although yessotoxin production has been suggested for *P. saltonense*, as discussed by Mertens et al., 2018, p. 73, this needs further confirmation. This, in addition to low abundances of cells and cysts of *P. lapazense* in the Gulf of California, suggests that this species is not responsible for the observed yessotoxin concentrations in shellfish by Leyva-Valencia et al. (2021). The presence of yessotoxins could be related to other dinoflagellates reported in this bay such as *Lingulodinium polyedra* or *Gonyaulax spinifera* (Gárate-Lizárraga et al., 2014, Morquecho-Escamilla et al., 2016).

4.6. Cyst wall composition based on ATR micro-FTIR-spectroscopy

Average ATR micro-FTIR spectra from the species analyzed in this study (Fig. 16) strongly resemble previously published spectra of other gonyaulacalean dinocysts, i.e. recent *Lingulodinium machaerophorum* (Versteegh et al., 2012) and fossil *Thalassiphora pelagica* (~40 Ma, Rhine Graben, ~31 Ma, Kerguelen Plateau) (Versteegh et al., 2020). All spectra presented here show absorption bands which indicate a relatively short-chain aliphatic cyst wall macromolecule with primarily hydroxyl (mainly as H-bonds), ether and carbonyl groups (possibly as carboxylic acids) (Table 6).

Relative to the apex of the OH-band, the average *Operculodinium centrocarpum* spectrum generally shows stronger aliphatic (2934, 2859 and 1432 cm^{-1}), carbonyl (1700 cm^{-1}) and alkene (1647 cm^{-1}) peaks than in the average spectra of cysts of *Protoceratium reticulatum*, *Operculodinium lapazense* and other gonyaulacalean outgroups (Table 7). This could possibly be due to one or a combination of several of the following factors: (i) intrinsic – perhaps species-specific – variations in cyst wall macromolecules; (ii) differences in environmental conditions during cyst formation; (iii) post-mortem diagenetic alteration of the cyst wall macromolecules; (iv) condensation of cell content molecules onto the cyst interior; (v) externally added nonvisible contaminants and/or (vi) alteration of cyst wall macromolecules by strong acids (HCl + HF) during sample processing. More subtle differences between the average spectra of recent taxa (Fig. 16) might also, in part, be due to (some of) these factors. As the possible effects of these variables on the spectral outcomes is still largely unknown, it is difficult to pinpoint exactly which ones might have played a role here. On the other hand, ATR micro-FTIR spectra – as measured via the protocol used in this study – rather offer qualitative information (i.e. absorption band positions in terms of wavenumbers) over quantitative, as several experimental parameters can slightly influence the (relative) heights of absorption bands (Meyvisch et al., 2021). Thus, extra care should be

taken when making detailed interpretations on generally subtle intensity differences. All gonyaulacalean spectra presented here are highly comparable, suggesting very similar cyst wall compositions, which falls in line with previous FTIR studies (Bogus et al., 2014, Versteegh et al., 2020).

Acknowledgements

The Regional Council of Brittany, the General Council of Finistère and the urban community of Concarneau-Cornouaille-Agglomération are acknowledged for the funding of the Sigma 300 FE-SEM of the station of Marine Biology in Concarneau. Oury Teboulle is gratefully acknowledged for help obtaining topotype material from the Geological Survey of Israel (GSI). This study was also supported by CIBNOR project 20449, and CONACYT A1-S-37026 grant. Amada Reyes-Salinas (CIBNOR) provided technical assistance. Thelma Castellanos and Angel Carrillo (CIBNOR) provided technical advice and infrastructure of the Molecular Microbial Ecology Laboratory. The project was partially funded by Instituto Politécnico Nacional, Mexico (grants SIP-20180551 and SIP-20220515). IGL is a COFAA fellow. Two anonymous reviewers are acknowledged for comments that significantly improved the manuscript.

Reference list

Andersen, R.A., Kawachi, M., 2005. Traditional microalgae isolation techniques. In : Andersen, R.A. (Ed.), Algal culturing techniques. Elsevier Academic Press, Burlington, MA, pp. 83–100.

Anderson, D.M., Kulis, D. M., Binder, B.J., 1984. Sexuality and cyst formation in the dinoflagellate *Gonyaulax tamarensis*: cyst yield in batch cultures. J. Phycol. 20, 418–425.

Antoine, E., Fleurence, J., 2003. Species identification of red and brown seaweeds using ITS ribosomal DNA amplification and RFLP patterns. J. Sci. Food Agric. 83, 709–713.

Band-Schmidt, C.J., Bustillos-Guzmán, J.J., López-Cortés, D.J., Núñez-Vázquez, E., Hernández-Sandoval, F.E., 2011. El estado actual del estudio de florecimientos algales nocivos en México. Hidrobiológica 21 (3), 381–413.

Boc, A., Diallo, A.B., Makarenkov, V., 2012. T–REX: a web server for inferring, validating and visualizing phylogenetic trees and networks. Nucleic Acids Res. 40 (W1), W573–W579.

Bogus, K., Mertens, K.N., Lauwaert, J., Harding, I.C., Vrielinck, H., Zonneveld, K.A.F., Versteegh, G.J.M., 2014. Differences in the chemical composition of organic-walled dinoflagellate resting cysts from phototrophic and heterotrophic dinoflagellates. J. Phycol. 50(2), 254–266.

Bolch, C.J.S., 1997. The use of polytungstate for the separation and concentration of living dinoflagellate cysts from marine sediments. Phycologia 37, 472–478.

Byrne, R., Mudie, P., Soutar, A., 1990. A pollen/dinoflagellate chronology for DSDP site 480, Gulf of California. In: Betancourt, J.L., MacKay, A.M. (Eds.), Proceedings of the 6th annual PACLIM workshop, March 5–8, 1989, vol. 23, Interagency ecological studies program for the Sacramento-San Joaquin Estuary, Tuscon, Arizona, pp. 105–110.

Carbonell-Moore, M.C., Mertens, K.N., 2019. Should *Gonyaulax hyalina* and *Gonyaulax fragilis* (Dinophyceae) remain two different taxa? Phycologia 58(6), 685–689.

Carbonell-Moore, C., Mertens, K.N., 2020. On *Acanthogonyaulax spinifera* (Dinophyceae). Phycologia 59, 456–459.

Carbonell-Moore, M.C., Matsuoka, K., Mertens, K.N., 2022. Gonyaulacalean tabulation revisited using plate homology and plate overlap, with emphasis on the ventral area (Dinophyceae). Phycologia 61, 195–210.

Coates, J., 2000. Interpretation of Infrared Spectra, A Practical Approach. In: Meyers, R.A., Ed., Encyclopedia of Analytical Chemistry, John Wiley & Sons Ltd., Chichester, 10881–10882.

Chomérat, N., Couté, A. 2008. *Protoperidinium bolmonense* sp. nov. (Peridiniales, Dinophyceae), a small dinoflagellate from a brackish hypereutrophic lagoon (South of France). Phycologia 47, 392–403.

Chomérat, N., Sellos, D.Y., Zentz, F. Nézan E., 2010. Morphology and molecular phylogeny of *Prorocentrum consutum sp. nov*. (Dinophyceae), a new benthic dinoflagellate from south Brittany (northwestern France). J. Phycol 46, 183–194.

Colthup, N.B., Daly, L.H., Wiberley S.E., 1990. Introduction to Infrared and Raman Spectroscopy. Boston: Academic Press.

Couté, A., 2002. Biologie et microscopie électronique à balayage. Mémoires de la Société Entomologique de France 6, 31–44.

Davey, R.J., Downie, C., Sarjeant, W.A.S., Williams, G.L., 1966. VII. Fossil dinoflagellate cysts attributed to *Baltisphaeridium*. In: Davey, R.J., Downie, C., Sarjeant, W.A.S. and Williams, G.L. (Eds.), Studies on Mesozoic and Cainozoic dinoflagellate cysts; British Museum (Natural History) Geology, Bulletin, Supplement 3, p. 157-175.

Doblin, M., Blackburn, S.I., Hallegraeff, G.M., 1999. Comparative study of selenium requirements of three phytoplankton species: *Gymnodinium catenatum*, *Alexandrium minutum* (Dinophyta) and *Chaetoceros* cf. *tenuissimus* (Bacillariophyta). J. Plankton Res. 21, 1153–1169.

Dodge, J.D., 1988. An SEM study of thecal division in *Gonyaulax* (Dinophyceae). Phycologia 27, 241–247.

Downie, C, Sarjeant, W.A.S., 1965. Bibliography and index of fossil dinoflagellates and acritarchs. Geological Society of America, Memoir 94, p. 1–180.

Fensome, R.A., Taylor, F.J.R., Norris, G., Sarjeant, W.A.S., Wharton, D.I., Williams, G.L., 1993. A classification of fossil and living dinoflagellates. Micropaleontology Press Special Paper, no.7, 351 p.

Gárate-Lizárraga, I., Hernández-Orozco, M.L., Band-Schmidt, C.J, Serrano-Casillas, G., 2001. Red tides along the coasts of Baja California Sur, Mexico (1984–2001). Oceánides 16, 127–134.

Gárate-Lizárraga, I., Muñeton-Gomez, M.S., Pérez-Cruz, B., Díaz-Ortiz, J.A., 2014. Bloom of *Gonyaulax spinifera* (Dinophyceae: Gonyaulacales) in Ensenada de la Paz lagoon, Gulf of California. CICIMAR Oceánides 29(1), 11–18.

Gárate-Lizárraga, I., Okolodkov, Y.B., Cortés-Altamirano, R., 2016. Microalgas formadoras de florecimientos algales en el Golfo de California. In: García-Mendoza, E., Quijano-Scheggia, S.I., Olivos-Ortíz, A., Núñez-Vázquez, E.J. (Eds.), Florecimientos Algales Nocivos en México. CICESE, Ensenada, Baja California, México, pp. 130–145. [In Spanish]

Gómez-Valdés, J.G., Delgado, J.A., Dworak, J.A., 2003. Overtides, compound tides, and tidal residual current in Ensenada de la Paz lagoon, Baja California Sur. Mexico. Geofís. Intern. 42, 623–634.

Gu, H., Huo, K., Krock, B., Bilien, G., Luo, Z., Pospelova, V., Li, Z., Carbonell-Moore, C., Morquecho, L., Ninčević, Ž., Mertens, K.N., 2021. Cyst-theca relationships of *Spiniferites bentorii*, *S. hyperacanthus*, *S. ramosus*, *S. scabratus* and molecular phylogenetics of *Spiniferites* and *Tectatodinium* (Gonyaulacales, Dinophyceae). Phycologia 60(4), 332–353.

Guillard, R.R.L., Ryther, U.H., 1962. Studies on marine planktonic diatoms *Cyclotella nana* Hustedt and *Detonula confervaceae* (Cleve). Gran. Can. J. Microbiol. 8, 229–239.

Halfar, J., Godinez-Orta, L. Mutti, M., Valdez-Holguin, J.E., Borges, J.M.. 2006. Carbonates calibrated against oceanographic parameters along a latitudinal transect in the Gulf of California, Mexico. Sedimentology 53, 297–320.

Head, M.J., 1996. Late Cenozoic dinoflagellates from the Royal Society borehole at Ludham, Norfolk, eastern England. J. Paleontol. 70(4), 543–570.

Hernández-Becerril, D.U., 1987. A checklist of planktonic diatoms and dinoflagellates from the Gulf of California. Nova Hedwigia 45, 237–261.

Hernández-Becerril, D.U., Alonso-Rodríguez, R., Álvarez-Góngora, C., Barón-Campis, S.A., Ceballos-Corona, G., Herrera-Silveira, J., Meave del Castillo, M.E., Juárez-Ruíz, N., Merino-Virgilio, F., Morales-Blake, A., Ochoa, J.L., Orellana-Cepeda, E., Ramírez-Camarena, C., Rodríguez-Salvador, R., 2007. Toxic and harmful marine phytoplankton and microalgae (HABs) in Mexican Coasts. J. Environ. Sci. Health A., Part A: Toxic/Hazardous Substances and Environmental Engineering 42(10), 1349–1363.

Issar, A., 1961. Geology of the subterranean water horizons of the Shefela and the Sharon regions. Ph.D. Thesis, Geol. Surv. Israel [Jerusalem Hebrew with English Summ.].

Jansson, I., M., Mertens, K.N., Head, M.J., 2014. Statistically assessing the regional correlation between salinity and morphology in cysts produced by the dinoflagellate *Protoceratium reticulatum*. Paleogeography, Paleoclimatology, Palaeoecology 399, 202–213.

Kar, R.K., 1985. The fossil floras of Kachchh-IV. Tertiary palynostratigraphy. The Palaeobotanist 34, 1–280.

Katoh, K., Standley, D.M., 2013. MAFFT multiple sequence alignment software version 7: improvements in performance and usability. Mol. Biol. Evol. 30(4), 772–780.

Kofoid, C.A., Michener, J.R., 1911. New genera and species of dinoflagellates. Bull. Mus. Comp. Zool. 54(7), 267–302.

Lassus, P., Chomérat, N., Hess, P., Nézan, E., 2016. Toxic and Harmful Microalgae of the World Ocean / Micro-algues toxiques et nuisibles de l'océan mondial. International Society for the Study of Harmful Algae / Intergovernmental Oceanographic Commission of UNESCO, Denmark IOC Manuals and Guides, 68 [Bilingual English/ French].

Lechuga-Devéze, C.H., Morquecho-Escamilla, M.L., Reyes-Salinas, A., Hernández-Alfonso J.R., 2000. Environmental natural disturbances at Bahía Concepción, Gulf of California. In: Munawar, M., Lawrence, S.G., Munawar, I.F., Malley, D.F. (Eds.), Aquatic Ecosystems of Mexico: Status and Scope. Ecovision World Monographs Series, Backhuys Publishers, Leiden, The Netherlands, pp. 245–255.

Lentin, J.K., Williams, G.L., 1993. Fossil dinoflagellates: index to genera and species. 1993 edition. American Association of Stratigraphic Palynologists, Contributions Series 28, 856 + viii p.

Leyva-Valencia, I., Hernández-Castro, J.E., Band-Schmidt, C.J., Turner, A.D., O'Neill, A., Núñez-Vázquez, E.J., López-Cortés, D.J., Bustillos-Guzmán, J.J., Hernández-Sandoval, F.E., 2021. Lipophilic Toxins in Wild Bivalves from the Southern Gulf of California, Mexico. Marine Drugs 19 (2), 99.

Licea, S., Moreno, J.L., Santoyo, H., Figueroa, G., 1995. Dinoflageladas del Golfo de California. Universidad Autónoma de Baja California Sur, SEP-FOMES, PROMARCO. México, p. 165.

Limoges, A., Kielt, J. F., Radi, T., Ruiz-Fernandez, A.C., de Vernal, A., 2010. Dinoflagellate cyst distribution in surface sediments along the south-western Mexican coast (14.76°N to 24.75°N). Mar. Micropaleontol. 76(3–4), 104–12[illegible]

Limoges, A., Van Nieuwenhove, N., Head, M.J., Mertens, K.N., Pospelova, V., Rochon, A., 2020. A review of rare and less well known extant marine organic-walled dinoflagellate cyst taxa of the orders Gonyaulacales and Suessiales from the Northern Hemisphere. Mar. Micropaleontol. 159, 101801.

Loeblich, A.R., III, Indelicato, S.R., 1986. Thecal analysis of the tropical benthic dinoflagellate *Gambierdiscus toxicus*. Mar. Fish. Rev. 48, 38–43.

López-Cortés, D.J, Gárate-Lizárraga, I., Bustillos-Guzmán, J.J., Alonso-Rodríguez, R., Murillo-Murillo, I., 2003. Variabilidad del estado trófico y la biomasa de fitoplancton de Bahía Concepción, Golfo de California (1997–1999). Hidrobiológica 13, 195–206.

Luo, Z., Lim, Z.F., Mertens, K.N., Krock, B. Teng, S.T., Tan, T.H., Leaw, C.P., Lim, P.T., Gu, H., 2020. Attributing *Ceratocorys*, *Pentaplacodinium* and *Protoceratium* to Protoceratiaceae (Dinophyceae), with descriptions of *Ceratocorys malayensis sp. nov*. and *Pentaplacodinium usupianum sp. nov*. Phycologia 59(1), 6–23.

Martínez-Hernández, E., Hernández-Campos, E., 1991. Distribución de quistes de dinoflagelados y acritarcas en sedimentos holocénicos del Golfo de California. Paleontol. Mex. 57, p. 133.

Mertens, K.N., Ribeiro, S., Bouimetarhan, I., Caner, H., Combourieu Nebout, N., Dale, B., de Vernal, A., Ellegaard, M., Filipova, M., Godhe, A., Goubert, E., Grøsfjeld, K., Holzwarth, U., Kotthoff, U., Leroy, S.A.G., Londeix, L., Marret, F., Matsuoka, K., Mudie, P.J., Naudts, L., Peña-Manjarrez, J.L., Persson, A., Popescu, S.-M., Pospelova, V., Sangiorgi, F., van der Meer, M., Vink, A., Zonneveld, K.A.F., Vercauteren, D., Vlassenbroeck, J., Louwye, S., 2009. Process length variation in cysts of a dinoflagellate, *Lingulodinium machaerophorum*, in surface sediments: Investigating its potential as salinity proxy. Mar. Micropaleontol. 70(1–2), 54–69.

Mertens, K.N., Price, A., Pospelova, V., 2012a. Determining the absolute abundance of dinoflagellate cysts in recent marine sediments II: further tests of the *Lycopodium* marker-grain method. Rev. Palaeobot. Palynol. 184, 74–81.

Mertens, K.N., Bringué, M., Van Nieuwenhove, N., Takano, Y., Pospelova, V., Rochon, A., de Vernal, A., Radi, T., Dale, B., Patterson, R.T., Weckström, K., Andrén, E., Louwye, S., Matsuoka, K., 2012b. Process length variation of the cyst of the dinoflagellate *Protoceratium*

reticulatum in the North Pacific and Baltic-Skagerrak region: calibration as an annual density proxy and first evidence of pseudo-cryptic speciation. J. Quat. Sci. 27(7), 734–744.

Mertens, K.N., Wolny, J., Carbonell-Moore, C., Bogus, K., Ellegaard, M., Limoges, A., de Vernal, A., Gurdebeke, P., Omura, T., Al-Muftah, A., Matsuoka, K., 2015. Taxonomic re-examination of the toxic armoured dinoflagellate *Pyrodinium bahamense* Plate 1906: can morphology or LSU sequencing separate *P. bahamense* var. *compressum* from var. *bahamense*? Harmful Algae 41, 1–24.

Mertens, K.N., Carbonell-Moore, M.C., Pospelova, V., Head, M.J., Highfield, A., Schroeder, D., Gu, H., Andree, K.B., Fernandez, M., Yamaguchi, A., Takano, Y., Matsuoka, K., Nézan, E., Bilienm, G., Okolodkov, Y., Koike, K., Hoppenrath, M., Pfaff, M., Pitcher, G., Al-Muftah, A., Rochon, A., Lim P.T., Leaw, C.P., Lim, L.F., Ellegaard, M., 2018. *Pentaplacodinium saltonense* gen. et sp. nov. (Dinophyceae) and its relationship to the cyst-defined genus *Operculodinium* and yessotoxin-producing *Protoceratium reticulatum*. Harmful Algae 71, 57–77.

Mertens, K.N., Takano, Y., Meyvisch, P., Carbonell-Moore, M.C., Chomérat, N., Bogus, K., Leitão, M., 2021. Morpho-molecular and spectroscopic characterization of the freshwater dinoflagellate *Unruhdinium penardii* var. *robustum* (Kryptoperidiniaceae, Peridiniales), blooming in the Loir River, France. Nova Hedwigia 112(3–4), 283–306.

Meyvisch, P., Gurdebeke, P.R., Vrielinck, H., Mertens, K.N., Versteegh, G., Louwye, S., 2021. Attenuated Total Reflection (ATR) Micro-Fourier Transform Infrared (Micro-FT-IR)

Spectroscopy to Enhance Repeatability and Reproducibility of Spectra Derived from Single Specimen Organic-Walled Dinoflagellate Cysts. Appl. Spectrosc. 76 (2), 235–254.

Morquecho, L., Góngora-González, D.T., Okolodkov, Y.B., 2009. Cyst-theca relationships of Gonyaulacales and Peridiniales (Dinophyceae) from Bahía Concepción, Gulf of California. Acta Bot. Mex. 88, 9–29.

Morquecho, L., Lechuga-Devéze, C.H., 2003. Dinoflagellate cysts in recent sediments from Bahía Concepción, Gulf of California. Botanica Marina 46, 132–141.

Morquecho, L., Lechuga-Devéze, C.H., 2004. Seasonal occurrence of planktonic dinoflagellates and cyst production in relationship to environmental variables in subtropical Bahía Concepción, Gulf of California. Botanica Marina 47, 313–322.

Morquecho, L., Reyes-Salinas, A., 2004 onwards. Colección de Dinoflagelados Marinos (CODIMAR). Centro de Investigaciones Biológicas del Noroeste, S.C. La Paz, Baja California Sur, México. Accessed at http://www.cibnor.mx/investigacion/colecciones-biologicas/codimar el 2022/1/11

Morquecho-Escamilla, L., Reyes-Salinas, A., Okolodkov, Y.B., 2016. Illustrated Taxonomic Guide of the Marine Dinoflagellate Collection (CODIMAR). Scientific publication from the Centro de Investigaciones Biológicas del Noroeste, S.C.

Moshkovitz, S., 1961. The tracing of the Plio-Plesitocene boundary by means of Mollusca. Proc. Symp. Pleist. in Israel. Ass. Advancem. Sci & Israel Geol. Soc. [In Hebrew].

Moshkovitz, S., 1963. The Mollusca in the Upper part of the "Sakiebeds" (Upper Neogene Lower Pleistocene) in Central Coastal Plain of Israel. Israel. Journ. Earth Sci. 12(3), 97–146.

Muciño-Márquez, R.E., Gárate-Lizárraga, I., López-Cortés, D.J., Bustillos-Guzmán, J.J., Hernández-Sandoval, F.E., 2018. Seasonal variation of the phytoplankton community in tuna farms in Bahía de La Paz, southern gulf of California, Mexico. Lat. Am. J. Aquat. Res. 46, 1011–1024.

Nunn, G.B., Theisen, B.F., Christensen, B., Arctander, P., 1996. Simplicity-correlated size growth of the nuclear 28S ribosomal RNA D3 expansion segment in the crustacean order Isopoda. J. Mol. Evol. 42, 211–223.

Obeso-Nieblas, M., Alatorre-Mendieta, M.A., Jiménez-Illescas, A.R., 1996. Modelación de la marea en Bahía Concepción, B.C.S., México. CICIMAR Oceánides 11, 1–8.

Obeso-Nieblas, M., Gaviño-Rodríguez, J.H., Obeso-Huerta, H., 2012. Variabilidad espacial y estacional de temperatura, salinidad y densidad en Bahía Concepción, Golfo de California, México. Rev. Biol. Mar. Oceanogr. 47, 489–502.

Obeso-Nieblas, M., Shirasago-Germán, B., Gaviño-Rodríguez, J., Perez-Lezama, E., Obeso-Huerta, H., Jiménez-Illescas, A., 2008. Variabilidad hidrográfica en Bahía de La Paz, Golfo de California, México (1995-2005). Rev. Biol. Mar. Oceanogr. 43, 559–567.

Okolodkov, Y.B., Gárate-Lizárraga, I., 2006. An annotated checklist of dinoflagellates

(Dinophyceae) from the Mexican Pacific. Acta Bot. Mex. 74, 1–154.

Paz, B., Daranas, A.H., Norte, M., Riobó, P., Franco, J.M., Fernández, J.J., 2008. Yessotoxins, a group of marine polyether toxins: an overview. Mar. Drugs 6, 73–102.

Peña-Manjarrez, J.L., Helenes, J., Gaxiola-Castro, G., Orellano-Cepeda, E., 2005. Dinoflagellate cysts and bloom events at Todos Santos Bay, Baja California, México, 1999–2000. Cont. Shelf Res. 25, 1375–1393.

Posada, D., 2008. jModelTest: phylogenetic model averaging. Mol. Biol. Evol. 25(7), 1253–1256.

Pospelova, V., de Vernal, A., Pedersen, T. F. 2008. Distribution of dinoflagellate cysts in surface sediments from the northeastern Pacific (43–25°N) in relation to sea-surface conditions and upwelling, Mar. Micropaleontol. 68(1–2), 21–48.

Price, A., Mertens, K.N., Pospelova V., Pedersen, T.F., Ganeshram, R.S., 2013. Late Quaternary climatic and oceanographic changes in the Northeast Pacific as recorded by dinoflagellate cysts from Guaymas Basin, Gulf of California (Mexico). Paleoceanography 28, 1–13.

Reiss, Z., Issar, A., 1961. Contributions to the study of the Pleistocene in the Coastal Plain of Israel; Subsurface Quaternary correlation in Tel Aviv region. Bull. Geol. Surv. Israel. 32, 10–26.

Ronquist, F., Huelsenbeck, J.P., 2003. MrBayes 3: Bayesian phylogenetic inference under mixed models. Bioinformatics 19(12), 1572–1574.

Rossignol, M., 1962. Analyse pollinique de sédiments marins quaternaires en Israël II. - Sédiments pleistocènes. Pollen et Spores, 4(1), 121–148.

Rossignol, M., 1964. Hystrichosphères du Quaternaire en Méditerranée orientale, dans les sédiments Pléistocènes et les boues marines actuelles. Revue de micropaléontologie 7(2), 83–99.

Rubini, S., Albonetti, S., Menotta, S., Cervo, A., Callegari, E., Cangini, M., Dall'Ara, S., Baldini, E., Vertuani, S., Manfredini, S. 2021. New Trends in the Occurrence of Yessotoxins in the Northwestern Adriatic Sea. Toxins 13, 634.

Salgado, P., Figueroa, R.I., Ramilo, I., Bravo, I., 2017. The life history of the toxic marine dinoflagellate *Protoceratium reticulatum* (Gonyaulacales) in culture. Harmful Algae 68, 67–81.

Scholin, C.A., Herzog, M., Sogin, M., Anderson, D.M., 1994. Identification of group and strain-specific genetic markers for globally distributed *Alexandrium* (Dinophyceae). II. Sequence analysis of a fragment of the large subunit ribosomal RNA gene. J. Phycol. 30, 999–1011.

Stamatakis, A., 2006. RAxML–VI–HPC: maximum likelihood–based phylogenetic analyses with thousands of taxa and mixed models. Bioinformatics 22(21), 2688–2690.

Tillmann, U., Krock, B., Wietkamp, S., Beran, A., 2020. A Mediterranean *Alexandrium taylorii* (Dinophyceae) Strain Produces Goniodomin A and Lytic Compounds but Not Paralytic Shellfish Toxins. Toxins 12(9), 564.

Tillmann, U., Bantle, A., Krock, B., Elbrächter, M., Gottschling M., 2021. Recommendations for epitypification of dinophytes exemplified by *Lingulodinium polyedra* and molecular phylogenetics of the Gonyaulacales based on curated rRNA sequence data. Harmful Algae 104, 101956.

Thunell, R.C., Pride, C.J., Tappa, E., Muller- Karger, F.E., 1994. Biogenic silica fluxes and accumulation rates in the Gulf of California. Geol. 22, 303–306.

Toscano-Cepeda, A.E., Helenes, J., 2022. Oligocene–Miocene dinoflagellate cysts from the San Gregorio Formation, La Purísima area, Baja California Sur, Mexico. Palynology 46(1), 1–20.

Tubaro, A., Sosa, S., Carbonatto, M., Altinier, G., Vita, F., Melato, M., Satake, M., Yasumoto, Y., 2003. Oral and intraperitoneal acute toxicity studies of yessotoxin and homoyessotoxins in mice. Toxicon 41(7), 783–792.

Turland, N. J., Wiersema, J. H., Barrie, F. R., Greuter, W., Hawksworth, D. L., Herendeen, P. S., Knapp, S., Kusber, W.-H., Li, D.-Z., Marhold, K., May, T. W., McNeill, J., Monro, A. M., Prado, J., Price, M. J., Smith, G. F. (Eds.), 2018. International Code of Nomenclature for algae, fungi, and plants (Shenzhen Code) adopted by the Nineteenth International Botanical

Congress Shenzhen, China, July 2017. Regnum Vegetabile 159. Glashütten: Koeltz Botanical Books.

Van Nieuwenhove, N., Head, M.J., Limoges, A., Pospelova, V., Mertens, K.N., Matthiessen, J., De Schepper, S., de Vernal, A., Eynaud, F., Londeix, L., Marret, F., Penaud, A., Radi, T., Rochon, A., 2020. An overview and brief description of common marine organic-walled dinoflagellate cyst taxa occurring in surface sediments of the Northern Hemisphere. Mar. Micropaleontol. 159, 101814.

Verdugo-Díaz, G., 1997. Cambios estacionales del fitoplancton y de la composición bioquímica del material orgánico particulado en Bahía Concepción, B.C.S. Master's Thesis. Instituto Politécnico Nacional, Centro Interdisciplinario de Ciencias Marinas, La Paz, B.C.S., México. pp. 100.

Versteegh, G.J.M., Blokker, P., Bogus, K., Harding, I., Lewis, J., Oltmanns, S., Rochon, A., Zonneveld, K.A.F., 2012. Infrared spectroscopy, flash pyrolysis, thermally assisted hydrolysis and methylation (THM) in the presence of tetramethylammonium hydroxide (TMAH) of cultured and sediment-derived *Lingulodinium polyedrum* (Dinoflagellata) cyst walls, Org. Geochem. 43, 92–102.

Versteegh, G.J.M., Houben, A.J.P., Zonneveld, K.A.F., 2020. Better Molecular Preservation of Organic Matter in an Oxic Than in a Sulfidic Depositional Environment: Evidence from *Thalassiphora pelagica* (Dinoflagellata, Eocene) Cysts. Biogeosciences 17(13), 3545–3561.

Wall, D., 1967. Fossil microplankton in deep-sea cores from the Caribbean Sea. Palaeontology 10 (1), 95–123, pl. 14–16.

Wall, D., 1986. Dinoflagellate Cysts and Acritarchs from California Current Surface Sediments. PhD thesis, University of Saskatchewan.

Wall, D. and Dale, B., 1966. "Living fossils" in western Atlantic plankton. Nature 211 (5053), 1025–1026.

Wang, N., Mertens, K.N., Krock, B., Luo, Z., Derrien, A., Pospelova, V., Liang, Y., Bilien, G., Smith, K.F., De Schepper, S. Wietkamp, S., Tillmann, U., Gu, H., 2019. Cryptic speciation in *Protoceratium reticulatum* (Dinophyceae): evidence from morphological, molecular and ecophysiological data. Harmful Algae 88, 101610.

West, R.G., 1961. Vegetational history of the Early Pleistocene of the Royal Society Borehole at Ludham, Norfolk. Proc. R. Soc. B, 155, 437–453.

Williams, G.L., Fensome, R.A., MacRae, R.A., 2017. The Lentin and Williams index of fossil dinoflagellates 2017 edition. AASP Contributions Series 48, 1097 p.

Figure legends

Fig. 1. Map of the study areas indicating the location in the Gulf of California (A) of Bahía Concepción (B), Isla San José and Bahía de La Paz (C). Black dots indicate sample collection sites.

Fig. 2. (A) Living cyst isolated from sediment sample from Isla San José (ISJ-A-1 2014). (B–C) Same cyst as in (A) after hatching. (D) Cell hatched from the cyst shown in (A). (E–F) Cells of PEJV-4 strain, showing nucleus in E (denoted by arrow). All scale bars = 20 μm.

Fig. 3. (A–D, F) SEM micrographs of *Pentaplacodinium lapazense* (strain PEJV-3) and (E) from plankton (sample C). (A) Apical view (holotype). (B) Internal view of epitheca. (C) Antapical view with two antapicals. (D) Antapical view with one antapical. (E) Ventral view. (F) Dorsal view. Plate labels according to Kofoidian system. All scale bars = 10 μm.

Fig. 4. (A-F). SEM micrographs of sulcus of *Pentaplacodinium lapazense* (strain PEJV-3). Plate labels according to Kofoidian system. All scale bars = 2 μm.

Fig. 5. SEM micrographs of sulcus and apical pore complex (APC) of *Pentaplacodinium lapazense* (strains PEJV-3 and PEJV-4). (A–B). Sulcus (PEJV-3) (C, F, G) APC (PEJV-3). (D-E) APC (PEJV4). Plate labels according to Kofoidian system. All scale bars = 2 μm.

Fig. 6. Schematic line drawing of sulcus for *Pentaplacodinium lapazense*.

Fig. 7. (A–C). Fission line as observed in strain PEJV-4. All scale bars = 10 μm.

Fig. 8. Schematic line drawings of fission line (A,C) and plate overlap (B, D).

Fig. 9. SEM micrographs of *Operculodinium lapazense* cysts isolated from Isla San José surface sediment (ISJ A-5). (A). Typical shape of operculum. (B–E). Typical ornamentation of cyst wall. (F). Flagellar scar (denoted by arrow). Scale bars = 10 μm (A–B, E–F) or 2 μm (C, D).

Fig. 10. (A–F) Light microscope images of *Operculodinium lapazense* cyst isolated from sediment (ISJ B-1). (G–L) Light microscope images of *Operculodinium israelianum* from Reading 33/0 borehole, at 167 m depth below seafloor. All scale bars = 20 μm.

Fig. 11. Relation between average process lengths and body diameter for the three studied species.

Fig. 12. SEM micrographs of *Operculodinium israelianum* from Reading 33/0 at 167 m depth below seafloor. (A) Dorsal view showing archeopyle. (B) Same specimen as in A, but tilted. (C–E). Other specimens showing densely packed fibrils. Scale bars = 10 μm (A–B) or 2 μm (C–E).

Fig. 13. Light microscope micrographs of holotype of *Operculodinium saltonense* (Specimen on St. 5, slide 1 (UVic2013-271). (A) High focus showing dorsal view and archeopyle. (B) Mid focus showing wall cross section. (C). Low focus showing wall structure. All scale bars = 20 μm.

Fig. 14. LSU phylogeny. Phylogenetic tree inferred from Maximum likelihood (ML) based on the LSU rDNA (D1–D3) sequences. *Alexandrium margalefii* was chosen as the outgroup. Nodal labels in red indicate new strains and sequences obtained in this study. Branch lengths are drawn to scale, with the scale bar indicating the number of nucleotide substitutions per site. Nodal supports are bootstrap values of ML and Bayesian posterior probabilities (PP). Only ML values >50% and PP >0.8 are shown. Asterisk indicates ML bootstrap support value of 100% and a PP of 1.0.

Fig. 15. SSU phylogeny. Phylogenetic tree inferred from Maximum likelihood (ML) based on the SSU rDNA sequences. *Alexandrium affine* was chosen as the outgroup. Nodal labels in red indicate new strains and sequences obtained in this study. Branch lengths are drawn to scale, with the scale bar indicating the number of nucleotide substitutions per site. Nodal supports are bootstrap values of ML and Bayesian posterior probabilities (PP). Only ML values >50% and PP >0.8 are shown. Asterisk indicates ML bootstrap support value of 100% and a PP of 1.0.

Fig. 16. ITS phylogeny. Phylogenetic tree inferred from Maximum likelihood (ML) based on the ITS region sequences. *Tripos furca* was chosen as the outgroup. Nodal labels in red indicate new strains and sequences obtained in this study. Branch lengths are drawn to scale, with the scale bar indicating the number of nucleotide substitutions per site. Nodal supports are bootstrap values of ML and Bayesian posterior probabilities (PP). Only ML values >50% and PP >0.8 are shown. Asterisk indicates ML bootstrap support value of 100% and a PP of 1.0.

Fig. 17. Comparison of averaged and min-max normalized ATR micro-FTIR spectra from selected fossil and recent gonyaulacoid dinoflagellate cysts, including *Operculodinium lapazense*. Different line-types correspond to different samples. Diagnostic absorption peaks and shoulders are indicated with vertical dashed lines.

Abstract

A new *Pentaplacodinium* species with six precingular plates is described from Bahía Concepción and Bahía de la Paz, Gulf of California. The non-fossil motile stage is described as *Pentaplacodinium lapazense*, whilst the fossil stage is described as *Operculodinium lapazense*. The cyst morphology is compared to topotype material of *Operculodinium israelianum*, which is larger, has longer processes and has a different wall structure. The motile cells display a plate formula of Po, Pt, X, 2′+*2′, 6″, 6c, 7s, 5‴, 1p, 1⁗. A typical gonyaulacalean fission line and plate overlap are observed. SSU-ITS-LSU ribosomal DNA sequences demonstrate that *Pentaplacodinium saltonense* is its closest relative. The species is homothallic. This species occurs in relatively shallow and restricted coastal areas, and has a preference for higher sea-surface temperatures and salinities. MicroFTIR spectra of the cysts are compared to spectra of cysts of other gonyaulacaleans and suggest very similar compositions. No yessotoxins were detected in any of the analyzed strains, hence, this species is unlikely to be responsible for the elevated yessotoxin concentration observed in shellfish on the southern and central coastal region of the Gulf of California.

Author statement

Kenneth Neil Mertens and Lourdes Morquecho: Conceptualization, Methodology, Investigation, Original draft preparation, Writing, Reviewing and Editing. Consuelo Carbonell-Moore: Investigation, Original draft preparation, Writing, Reviewing and Editing. Pjotr Meyvisch: Methodology, Investigation, Writing, Reviewing and Editing. Haifeng Gu: Investigation, Writing, Reviewing and Editing. Gwenael Bilien: Investigation. Audrey Duval: Investigation. Amélie Derrien: Investigation, Writing, Reviewing and Editing. Vera Pospelova: Investigation, Writing, Reviewing and Editing. Kasia K. Śliwińska: Investigation. Ismael Gárate-Lizárraga: Investigation, Original draft preparation, Writing, Reviewing and Editing. Beatriz Pérez-Cruz: Investigation.

Declaration of interests

☒ The authors declare that they have no known competing financial interests or personal relationships that could have appeared to influence the work reported in this paper.

☐The authors declare the following financial interests/personal relationships which may be considered as potential competing interests:

Table 1. Strains of *Pentaplacodinium lapazense* established from vegetative cells and cyst germination, their locality, whether they were sequenced and analysed for toxins. Isla San José strains were established from vegetative cells (phytoplankton sample collected with a 20µm net): they are only four strains: PEJV-2, PEJV-3, PEJV-4, and PEJV-6, the letters "a" or "b" are the duplicates that were used for YST analysis. Bahía Concepción strains were established from cyst germinations; there are only two strains, PGCQ-1 and PGCQ-2, the letters "a" or "b" are the duplicates that were used for YST analysis. These were initially identified as *Protoceratium globosum* (Morquecho et al. 2009). LD = limit of detection (fg/cell), LQ = limit of quantification (fg/cell).

Strain name	Sampling date	Isolation date	Locality in the Gulf of California	Longitude	Latitude	Sequenced region	Yessotoxin analysis
PAZA 2 from ISJ-A-1 2014*	13/04/2014	21/02/2020	Isla San José	24°52' 28"N	110°32'53'W	SSU-ITS-LSU	NA
PEJV-2a	27/09/2011	30/09/2011	Isla San José	24° 52'31.82"N	110° 33'27.28"W	partial LSU (D1R-D3B)	NA
PEJV-3a	27/09/2011	30/09/2011	Isla San José	24° 52'31.82"N	110° 33'27.28"W	NA	<0.24 (LD), <0.72 (LQ)
PEJV-3b	27/09/2011	30/09/2011	Isla San José	24° 52'31.82"N	110° 33'27.28"W	partial LSU (D1R-D3B)	<0.28 (LD), <0.83 (LQ)
PEJV-4a	27/09/2011	30/09/2011	Isla San José	24° 52'31.82"N	110° 33'27.28"W	SSU-ITS-LSU	<0.18 (LD), <0.54 (LQ)
PEJV-4b	27/09/2011	30/09/2011	Isla San José	24° 52'31.82"N	110° 33'27.28"W	NA	<0.19 (LD), <0.57 (LQ)
PEJV-6a	27/09/2011	30/09/2011	Isla San José	24° 52'31.82"N	110° 33'27.28"W	partial LSU (D1R-D3B)	<0.57 (LD), <1.72 (LQ)
PEJV-6b	27/09/2011	30/09/2011	Isla San José	24° 52'31.82"N	110° 33'27.28"W	NA	<0.57 (LD), <1.70 (LQ)
PGCQ-1a	1/9/2002	Dec. 2002	Bahía Concepción	26°35'46.30"N	111°44'20.66"W	partial LSU (D1R-D3B)	<0.44 (LD), <1.31 (LQ)
PGCQ-1b	1/9/2002	Dec. 2002	Bahía Concepción	26°35'46.30"N	111°44'20.66"W	NA	<0.35 (LD), <1.06 (LQ)
PGCQ-1c	1/9/2002	Dec. 2002	Bahía Concepción	26°35'46.30"N	111°44'20.66"W	NA	NA
PGCQ-2a	1/9/2002	Dec. 2002	Bahía Concepción	26°35'46.30"N	111°44'20.66"W	NA	<0.23 (LD), <0.69 (LQ)
PGCQ-2b	1/9/2002	Dec. 2002	Bahía Concepción	26°35'46.30"N	111°44'20.66"W	NA	<0.20 (LD), <0.59 (LQ)

*This culture was hatched from a single cyst isolated from surface sediment.

Table 2. Oligonucleotide primers used for amplification.

Name	Target sequence	Direction	Sequence	Reference
18S-FW	SSU rDNA	Forward	TCCTGCCAGTAGTCATATGC	Chomérat et al. 2010
18S-RV	SSU rDNA	Reverse	TGATCCTTCGGCAGGTTCAC	Chomérat et al. 2010
ITS-FW	ITS1 – 5.8S rDNA – ITS2	Forward	GTAGGTGAACCTGCGGAAGG	Antoine and Fleurence 2003
D1R	LSU rDNA	Forward	ACCCGCTGAATTTAAGCATA	Scholin et al. 1994
D2C	LSU rDNA	Reverse	CCTTGGTCCGTGTTTCAAGA	Scholin et al. 1994
D3B	LSU rDNA	Reverse	TCGGAGGGAACCAGCTACTA	Nunn et al. 1996

Table 3. Background information on the samples and specimens analyzed via ATR micro-FTIR spectroscopy in this study.

Location	Labrador Sea (ODP, expedition 105, site 647, core 22, section [illegible], interval 0–7 cm)	Diana Lagoon, Corsica	Isla San José, Mexico
Latitude	53°19.876 'N	42°07.66' N	24°52' 28"N
Longitude	45°15.717 W	9°31.72' E	110°32'53'W
Sample type	Rock	Sediment	Sediment
Sampling method	Drill core	Hand sampling	Hand sampling
Water depth (m)	4071	1	8.5
Age	early Oligocene	Recent	Recent
Sampling date	17/10/1985	18/01/2016	13/04/2014
Taxon (nr. of specimens)	*Operculodinium centrocarpum* (4)	Cyst of *Protoceratium reticulatum* (2)	*Operculodinium lapazense* (2), *Spiniferites bentorii* (3) and *Polysphaeridium zoharyi* (10)
Sample processing	HCl (7.3%) + HF (40%)	No acids	HCl (?%)

procedure			
Picking procedure	Directly from processed residue	Directly from processed sediment	Directly from processed sediment

Table 4. Comparison between thecate morphologies of the six living species discussed here.

	Pentaplacodinium lapazense	*Pentaplacodinium saltonense*	*Pentaplacodinium usupianum*	*Protoceratium reticulatum*	*Protoceratium globosum*	*Ceratocorys malayensis*
Reference	This study	Mertens et al. (2018).	Luo et al. (2020).	Wang et al. (2019)	Kofoid and Michener (1911)	Luo et al. (2020).
Length	28.2 (41.4) 56.4 µm	37.8 (46.1) 59.8 µm	26.6–31.3 µm	25.4–47.4 µm	58 µm	40.2–58.0 µm
Width	28.2 (39.8) 56.4 µm	31.0 (39.5) 48.5 mm	22.7–27.7 µm	30.5–40.7 µm	52 µm	40.9–54.6 µm
Cingular displacement	1.0 widths	2.0 widths	1.0 widths	1.0 widths	?	2.0 widths
Ventral pore	Yes	Yes	None	Yes	?	Yes
Shape	Spherical	Spherical to slightly polyhedral	Elongated with antapical spines	Elongated, polyhedral	Spherical	Spherical with antapical spines
First apical plate	Insert with narrow contact	Insert with narrow contact	Insert with narrow contact	Insert with wide contact	?	Episert type 1
Pores	Yes	Yes	Yes	Yes	None	Yes
Precingular plates	6	5	6	6	?	6
Toxicity	No toxins found.	Potential yessotoxin producer.	No toxins found.	Potential yessotoxin producer.	Not known.	No toxins found.
Cyst equivalent	*Operculodinium lapazense*	*Operculodinium saltonense*	Not known.	*Operculodinium centrocarpum* sensu Wall and Dale 1966	Not known.	Not known.

Table 5: Strains analyzed for yessotoxin concentrations. Isla San José strains (PEJV) were established from vegetative cells. Bahía Concepción strains (PGCQ) were established from cyst germinations.

Strain replicates	Cells mL^{-1}	Culture volume (mL)	Number of cells in the pellet
PEJV-3a	311	40	12,440

Table 6.

PEJV-3b	270		10,800
PEJV-4a	414		16,560
PEJV-4b	397		15,880
PEJV-6a	131		5,240
PEJV-6b	132		5,280
PGCQ-1a	172		6,880
PGCQ-1b	212		8,480
PGCQ-2a	328		13,120
PGCQ-2b	384		15,360

Assignment of FTIR absorption bands from averaged ATR micro-FTIR spectra retrieved in this study.

Group frequency, Wavenumber (cm^{-1})	**Origin**	**Assignment**
3600–3200 (broad)	O-H	OH stretching
2936	C-H	Aliphatic CH_2 asymmetric stretching
2859	C-H	Aliphatic CH_2 symmetric stretching
1700	C=O	Carbonyl stretching (possibly from carboxylic acid)
1647	C=C	Alkene stretching
1593	C=C	Conjugated C=C stretching
1470–1410 (several)	C-H	Aliphatic CH_2 bending
1377	C-H	CH bending
1270–1200 (several)	C-O	C-O stretching
1141	C-O-C	Asymmetric ether stretching
1054	C-OR	Sugar ring stretching
975	C=C	Alkene bending
875	C-H	CH_2 vibration
795	C-H	$(CH_2)_n$-rocking ($n \geq 3$)
653	C-OH	Out-of-plane bending

Table 7. Relative intensities of aliphatic (2934, 2859 and 1432 cm^{-1}), carbonyl (1700 cm^{-1}) and alkene (1647 cm^{-1}) absorption peaks with respect to the apex of the OH-band (* 3385 cm^{-1} for

Operculodinium centrocarpum, 3335 cm^{-1} for other taxa), as calculated from the average ATR micro-FTIR spectra presented in Figure 16.

Taxon	$\frac{\mathbf{2934\ cm^{-1}}}{\mathbf{OH^*}}$	$\frac{\mathbf{2859\ cm^{-1}}}{\mathbf{OH^*}}$	$\frac{\mathbf{1432\ cm^{-1}}}{\mathbf{OH^*}}$	$\frac{\mathbf{1700\ cm^{-1}}}{\mathbf{OH^*}}$	$\frac{\mathbf{1647\ cm^{-1}}}{\mathbf{OH^*}}$
Operculodinium centrocarpum	0,70	0,44	0,37	0,53	0,56
Cyst of *Protoceratium reticulatum*	0,51	0,33	0,27	0,14	0,29
Operculodinium lapazense	0,64	0,45	0,31	0,24	0,22
Spiniferites bentorii	0,53	0,35	0,30	0,27	0,21
Polysphaeridium zoharyi	0,74	0,51	0,26	0,11	0,14

Table 8. Comparison between cyst morphologies of the three fossil species discussed here.

	Operculodinium lapazense	*Operculodinium salmonense*	*Operculodinium israelianum*
Maximum central body diameter	43.3 (50.6) 63.8 µm	48.6 (56.3) 70.9 mm	45.2 (56.4) 70.2 µm
Minimum central body diameter	42.5 (48.1) 57.8 µm	45.7 (52.1) 61.4 mm	41.4 (52.1) 66.4 µm
Process length	3.4 (5.4) 7.4 µm	1.0 (3.1) 5.7 mm	6.4 (10.5) 15.3 µm
Wall thickness	0.4 (1.4) 3.2 µm	0.9 (1.6) 2.4 µm	0.2 (1.2) 2.5
Flagellar scar	Yes	No	No
Packing of fibrils	Loose	Loose	Dense

Highlights

- A new species *Pentaplacodinium lapazense* is described from the southwestern coastal region of the Gulf of California, Mexico.
- The plate formula is: Po, Pt, X, 2′+*2′, 6″, 6c, 7s, 5‴, 1p, 1⁗.
- The corresponding cyst stage is similar to *Operculodinium israelianum* and is named *Operculodinium lapazense*.
- No yessotoxins were detected in the analyzed ten strains.


A
USA
Mexico
Gulf of California
Pacific Ocean
Mexico
N
Bahía Concepción
26°55'N
26°50'N
26°45'N
26°40'N
26°35'N
111°50'W
111°45'W
B
C
25°N
Isla San José
24°45'N
Bahía de La Paz
24°30'N
24°15'N
110°45'W
110°30'W

Figure 1

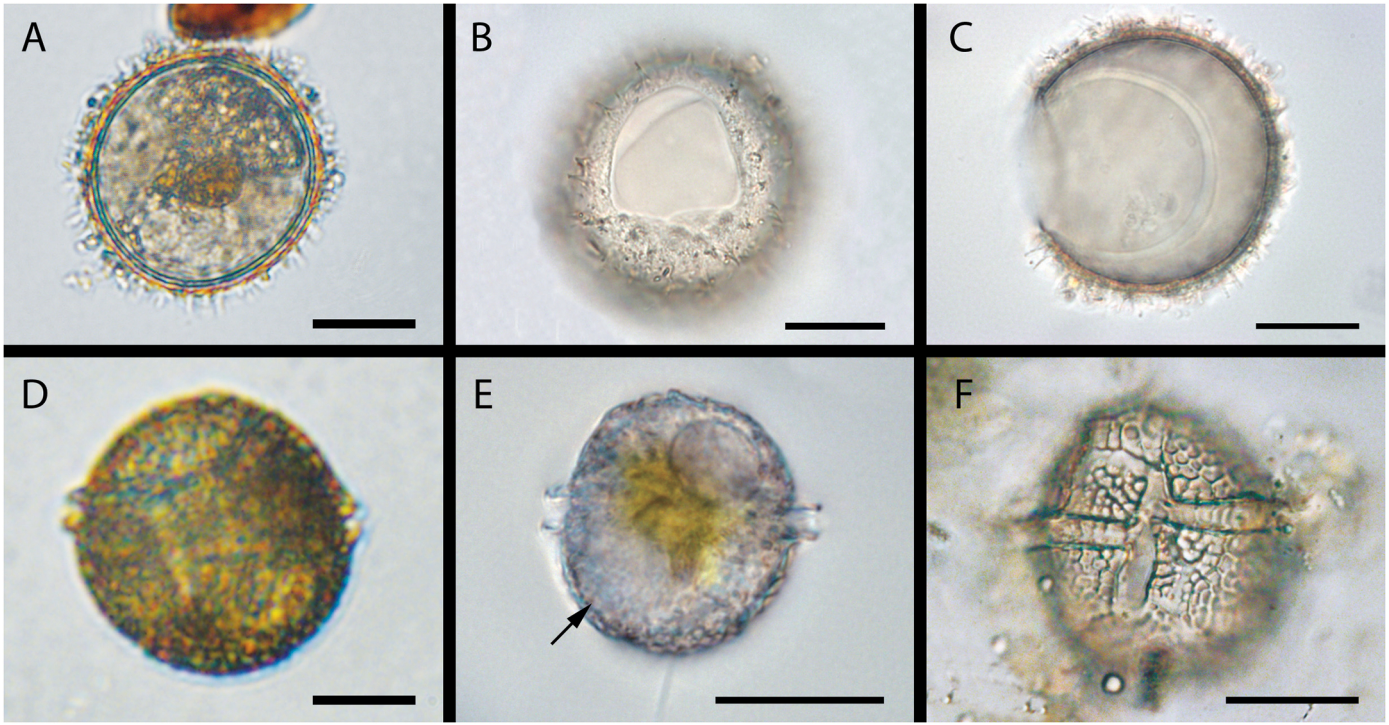

Figure 2

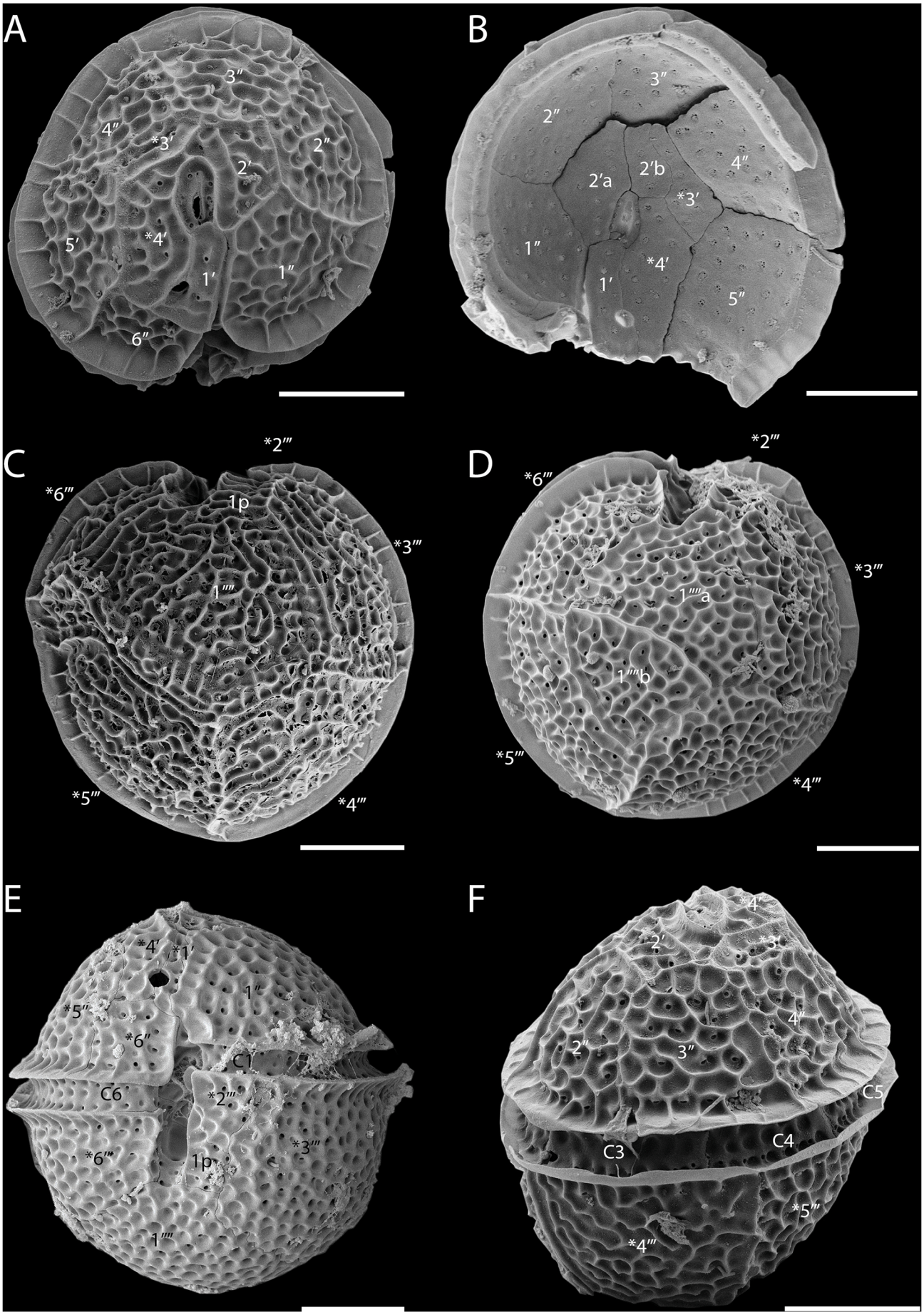
A
3″
4″
*3′
2″
2′
5′
*4′
1′
1″
6″
B
3″
2″
2′a
2′b
4″
*3′
1″
*4′
1′
5″
C
*2‴
*6‴
1p
*3‴
1⁗
*5‴
*4‴
D
*2‴
*6‴
*3‴
1⁗a
1⁗b
*5‴
*4‴
E
*4′
*1′
1″
*5″
*6″
C1
C6
*2‴
*3‴
*6‴
1p
1⁗
F
*4′
2′
*3′
4″
2″
3″
C5
C3
C4
*5‴
*4‴

Figure 3

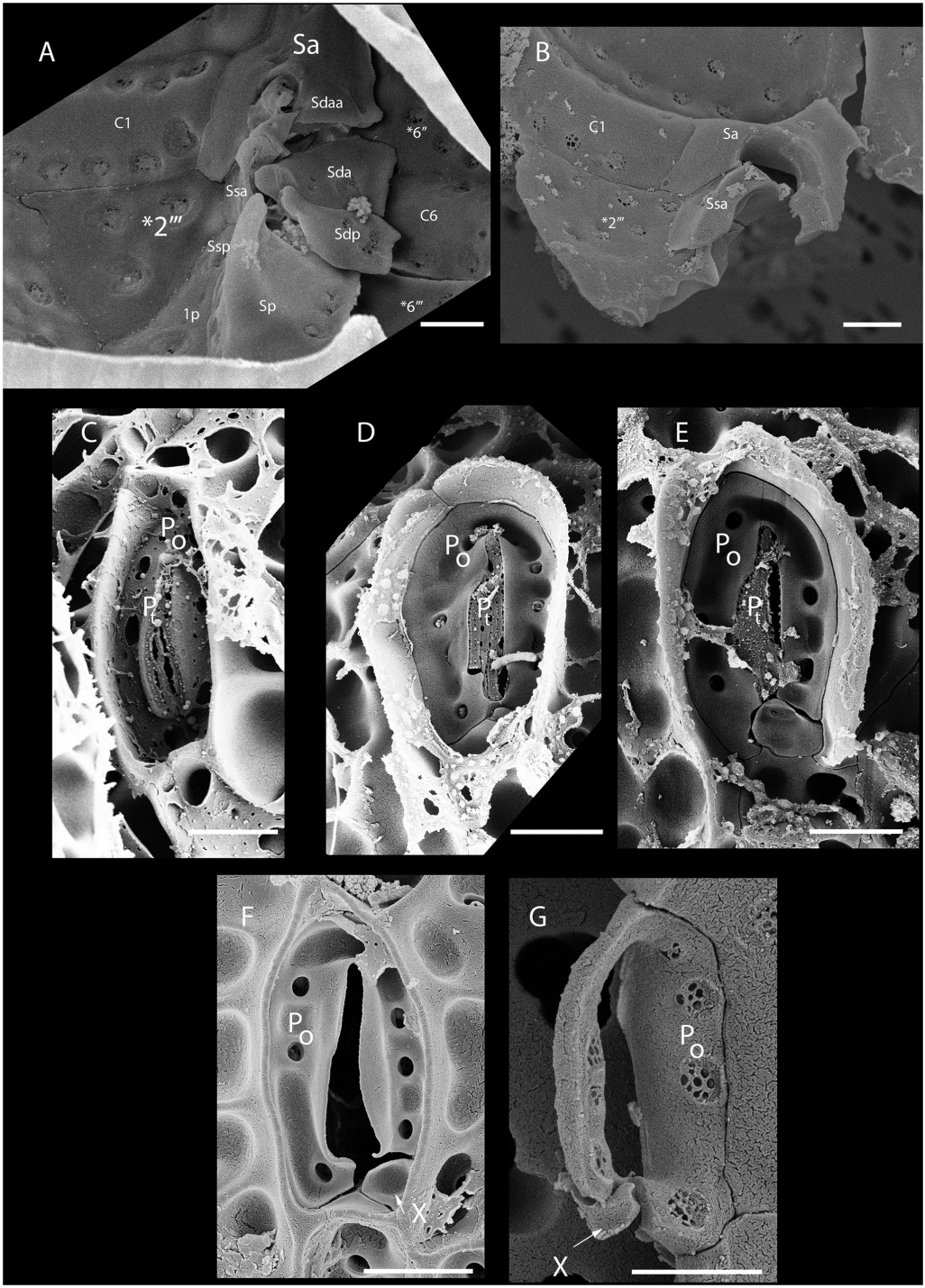
A
Sa
Sdaa
C1
*6″
Sda
Ssa
C6
*2‴
Sdp
Ssp
1p
Sp
*6‴
B
C1
Sa
Ssa
*2‴
C
Po
Pt
D
Po
Pt
E
Po
Pt
F
Po
X
G
Po
X

Figure 4

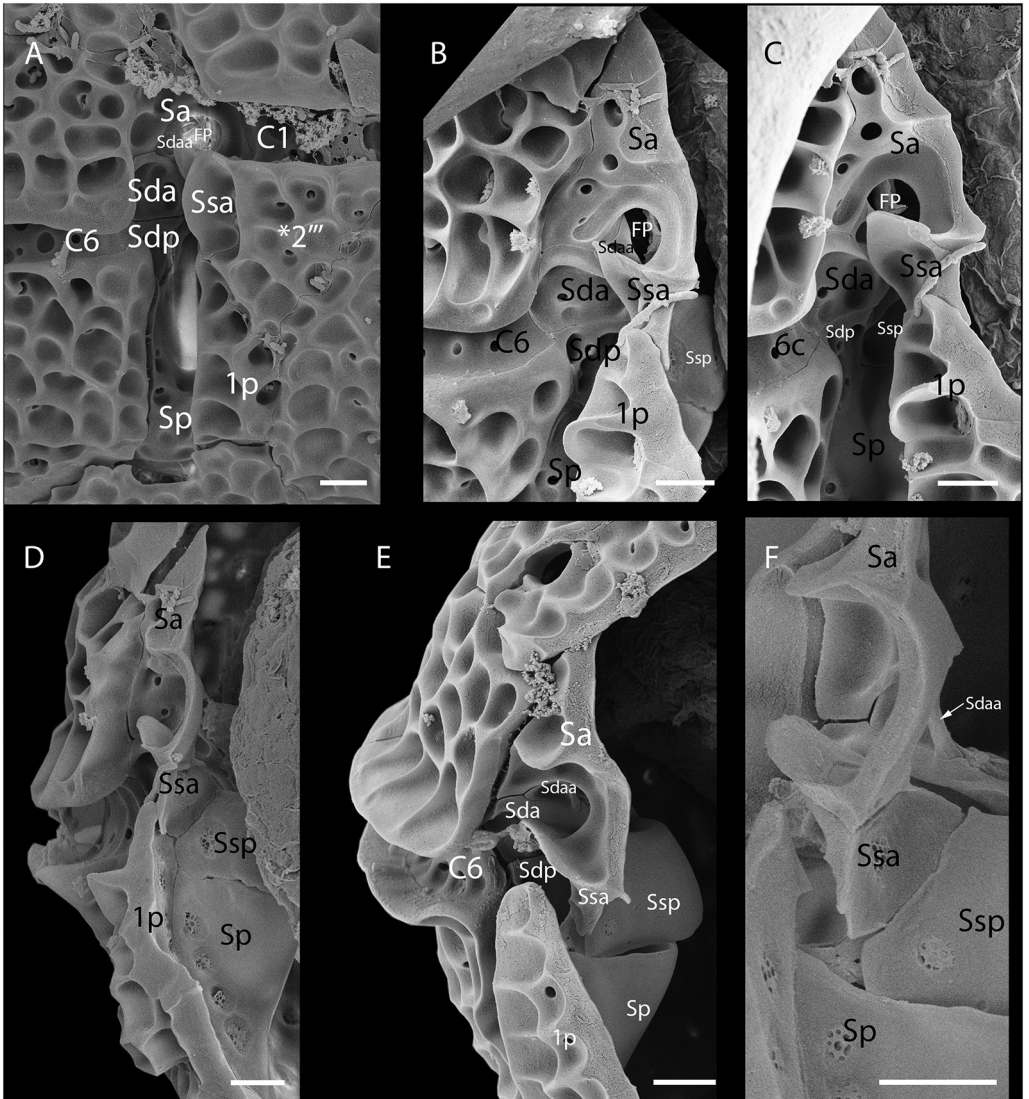
A
Sa
Sdaa
FP
C1
Sda
Ssa
C6
Sdp
*2‴
1p
Sp
B
Sa
FP
Sdaa
Sda
Ssa
C6
Sdp
Ssp
1p
Sp
C
Sa
FP
Sda
Ssa
6c
Sdp
Ssp
1p
Sp
D
Sa
Ssa
Ssp
1p
Sp
E
Sa
Sdaa
Sda
C6
Sdp
Ssa
Ssp
Sp
1p
F
Sa
Sdaa
Ssa
Ssp
Sp

Figure 5

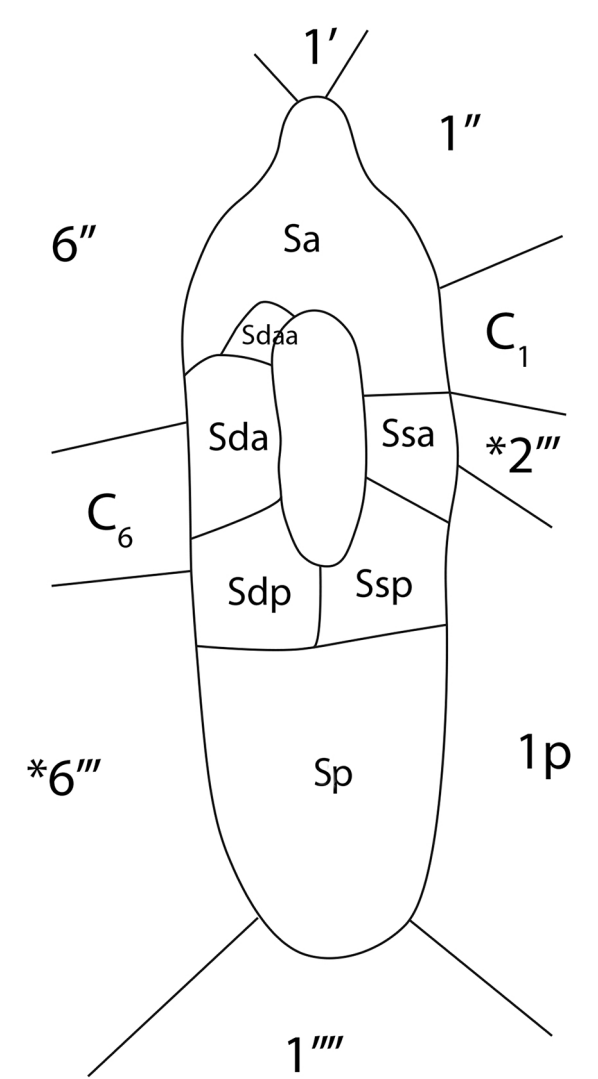

Figure 6

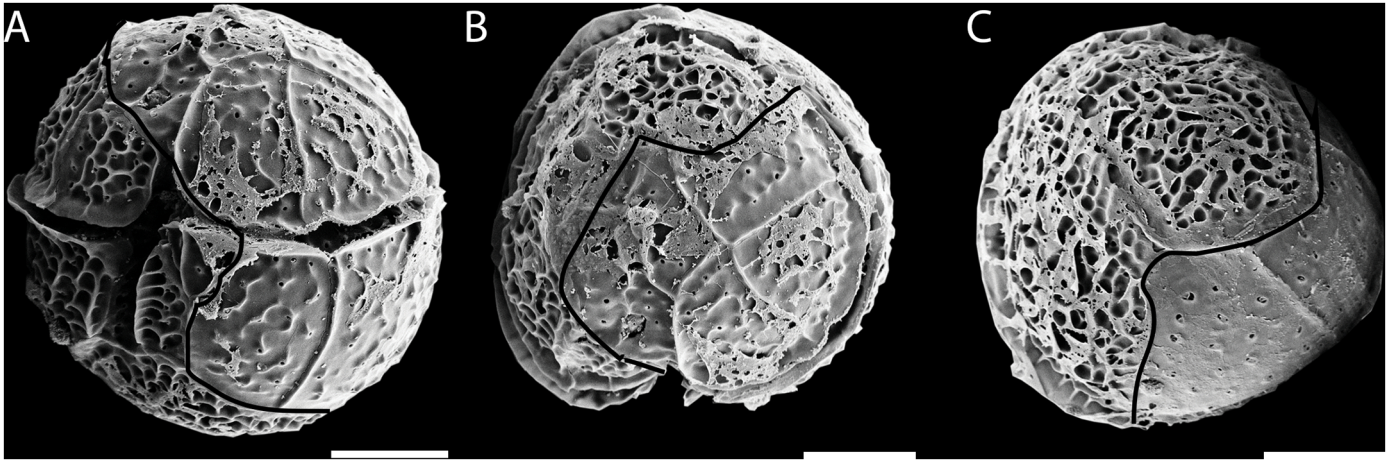

Figure 7

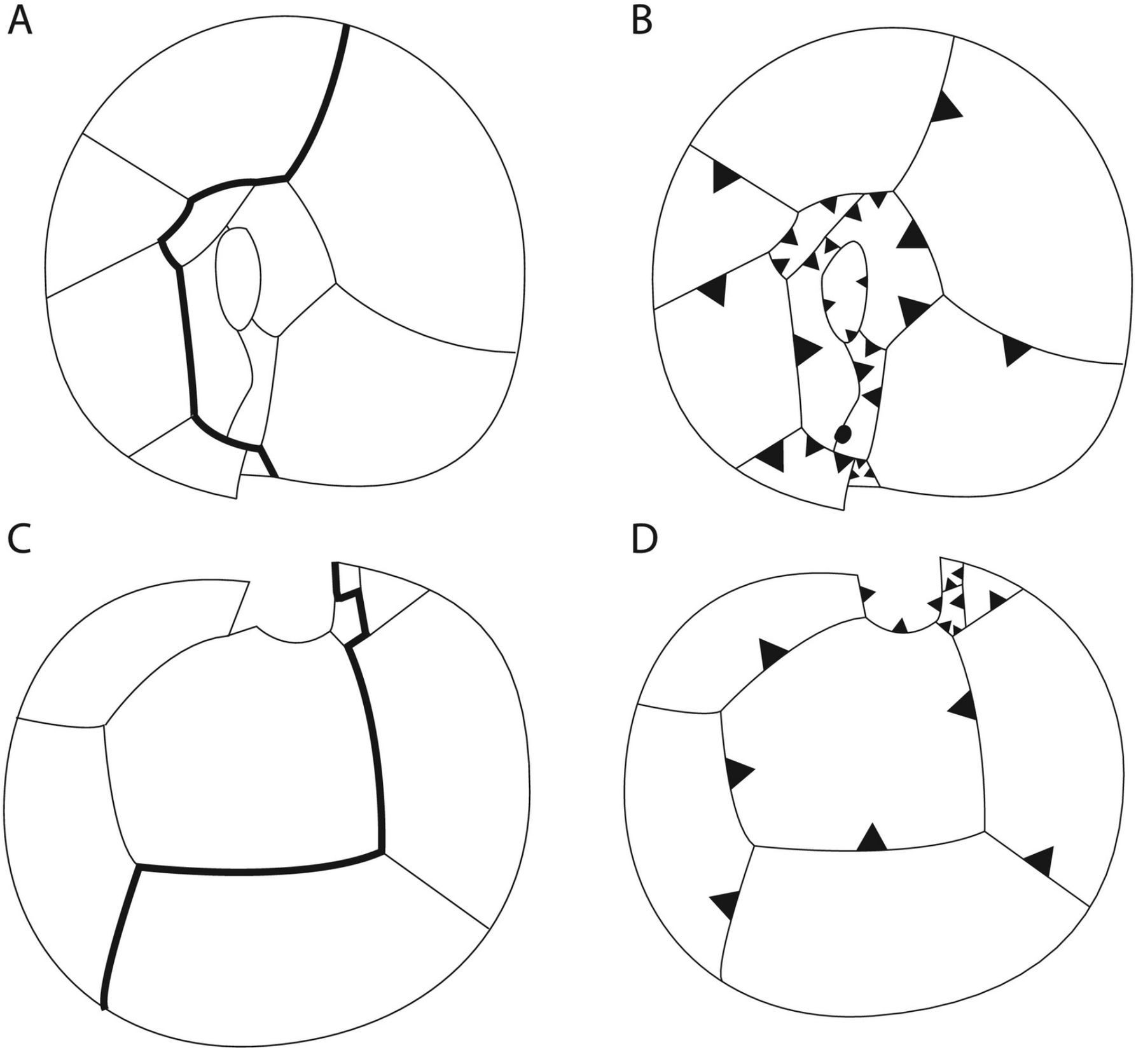

Figure 8

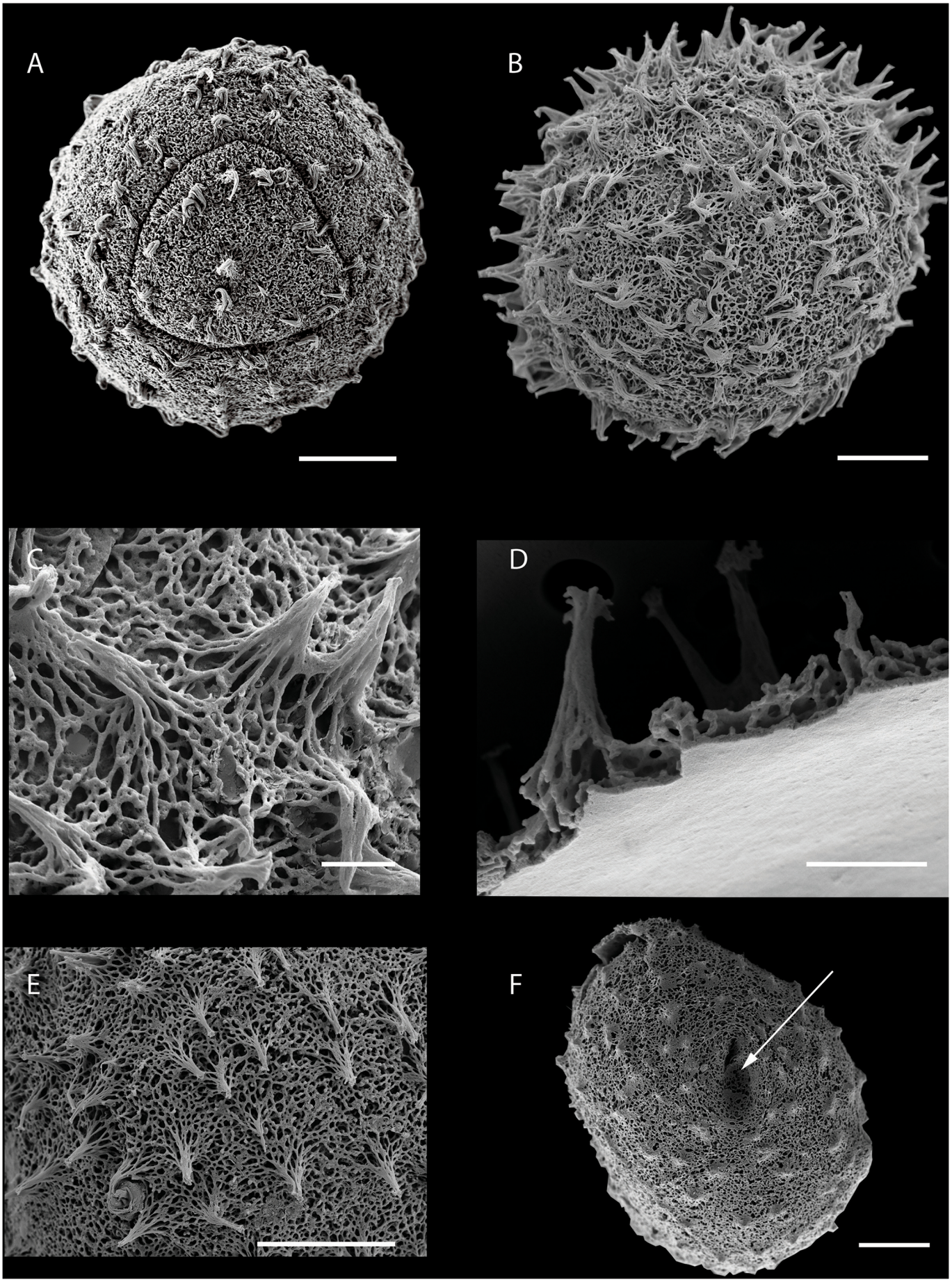

Figure 9

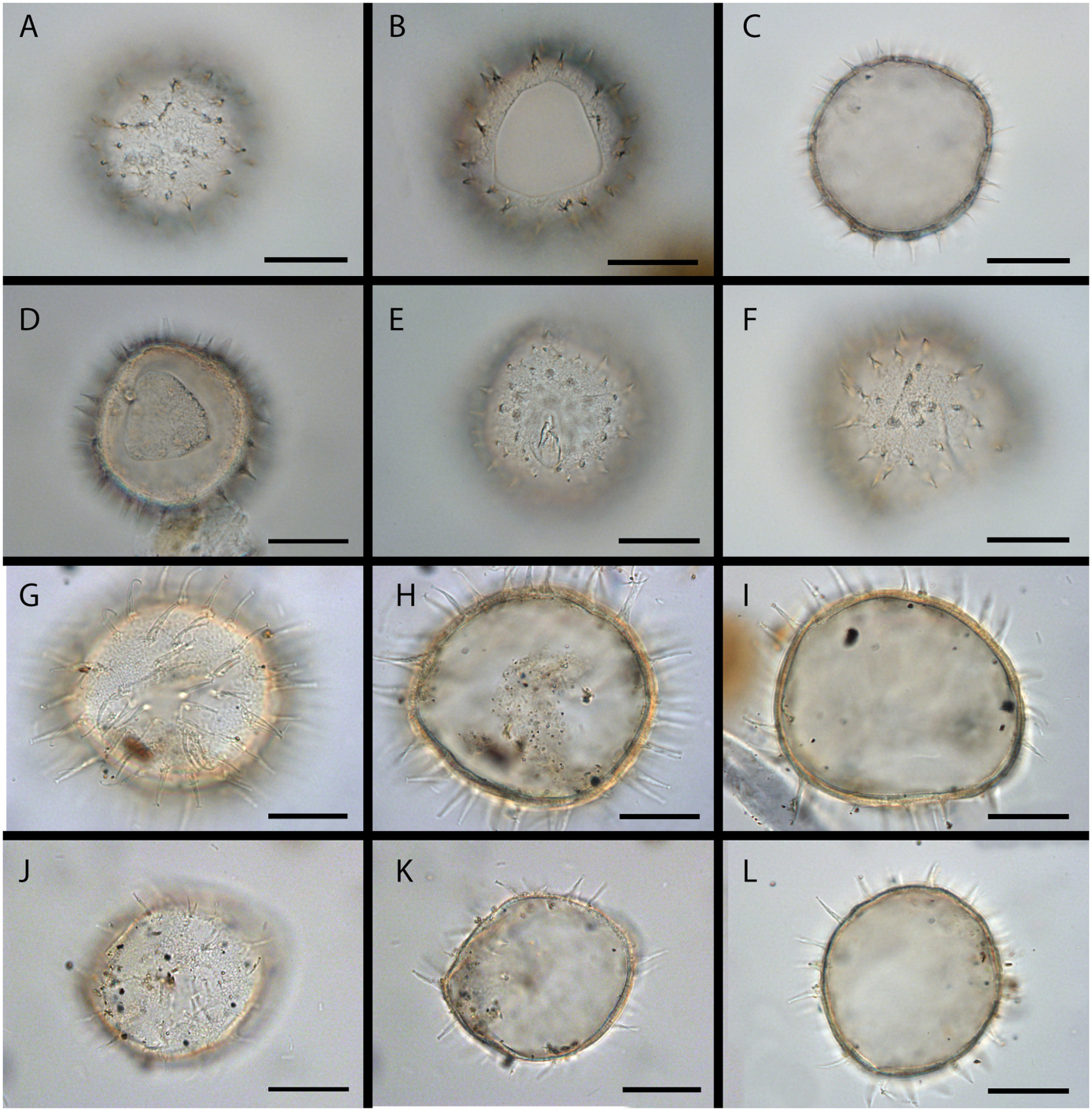

Figure 10

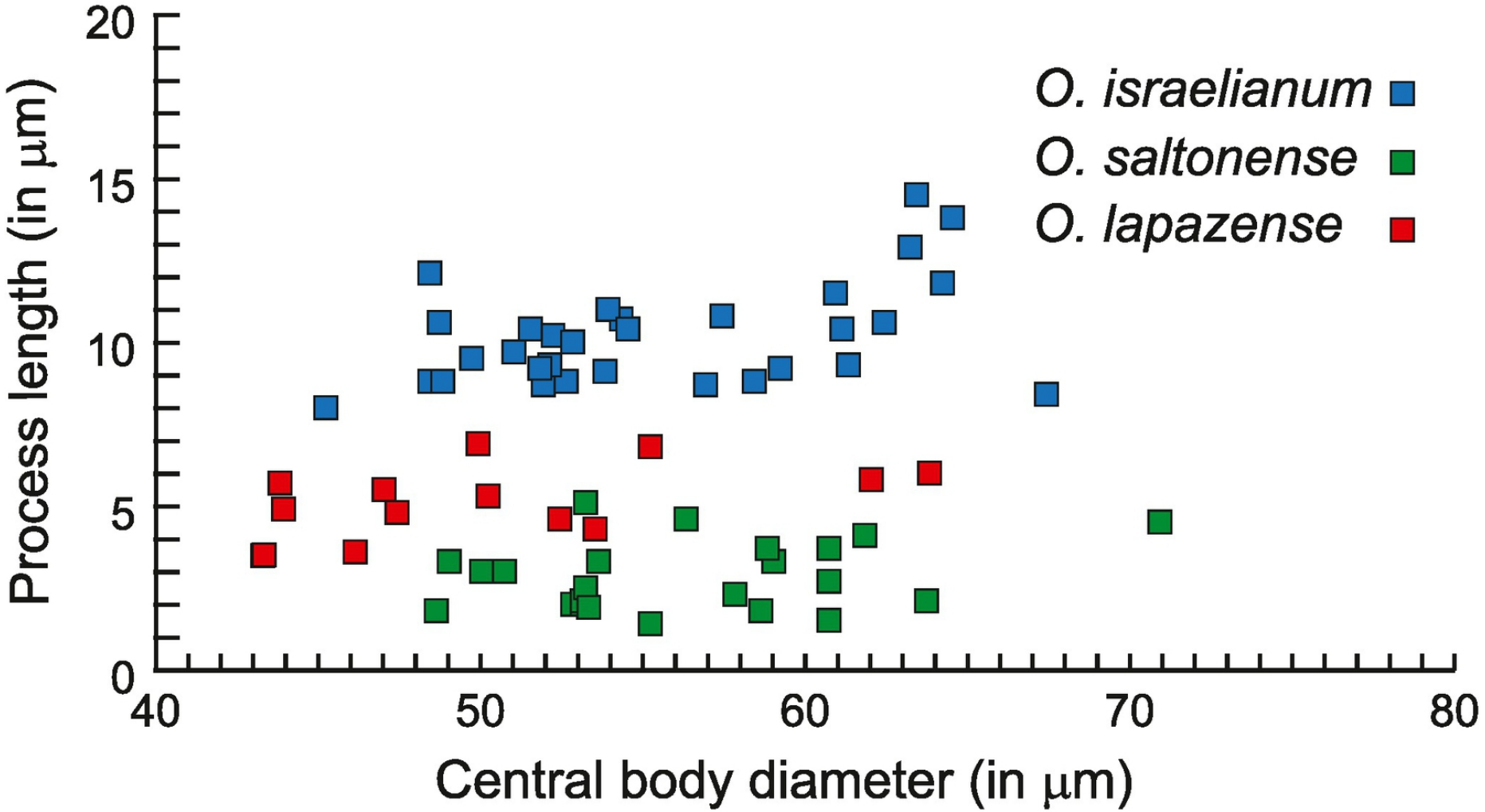
Process length (in μm)
20
15
10
5
0
40
50
60
70
80
Central body diameter (in μm)
O. israelianum
O. saltonense
O. lapazense

Figure 11

Figure 12

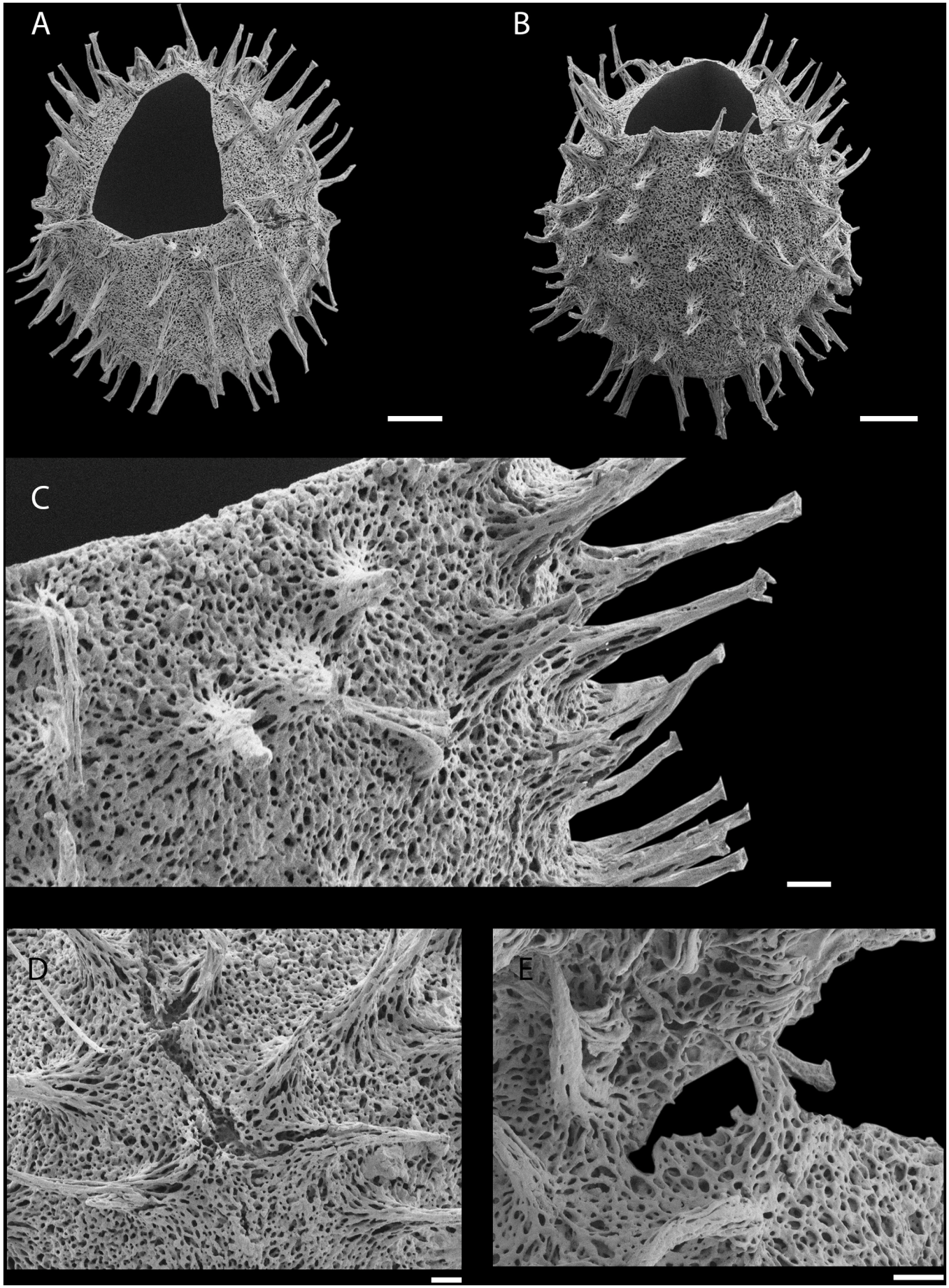

Figure 13

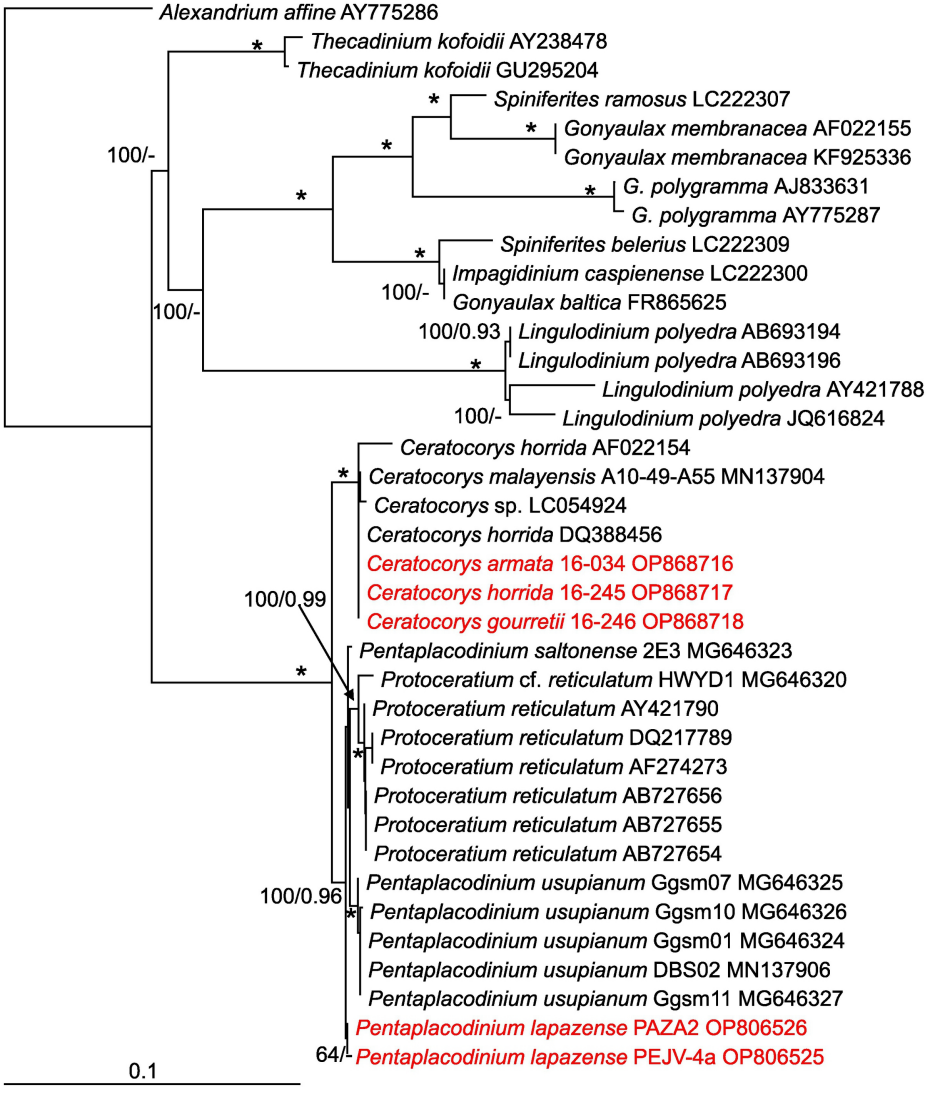
Alexandrium affine AY775286
Thecadinium kofoidii AY238478
Thecadinium kofoidii GU295204
Spiniferites ramosus LC222307
Gonyaulax membranacea AF022155
Gonyaulax membranacea KF925336
G. polygramma AJ833631
G. polygramma AY775287
Spiniferites belerius LC222309
Impagidinium caspienense LC222300
Gonyaulax baltica FR865625
Lingulodinium polyedra AB693194
Lingulodinium polyedra AB693196
Lingulodinium polyedra AY421788
Lingulodinium polyedra JQ616824
Ceratocorys horrida AF022154
Ceratocorys malayensis A10-49-A55 MN137904
Ceratocorys sp. LC054924
Ceratocorys horrida DQ388456
Ceratocorys armata 16-034 OP868716
Ceratocorys horrida 16-245 OP868717
Ceratocorys gourretii 16-246 OP868718
Pentaplacodinium saltonense 2E3 MG646323
Protoceratium cf. reticulatum HWYD1 MG646320
Protoceratium reticulatum AY421790
Protoceratium reticulatum DQ217789
Protoceratium reticulatum AF274273
Protoceratium reticulatum AB727656
Protoceratium reticulatum AB727655
Protoceratium reticulatum AB727654
Pentaplacodinium usupianum Ggsm07 MG646325
Pentaplacodinium usupianum Ggsm10 MG646326
Pentaplacodinium usupianum Ggsm01 MG646324
Pentaplacodinium usupianum DBS02 MN137906
Pentaplacodinium usupianum Ggsm11 MG646327
Pentaplacodinium lapazense PAZA2 OP806526
Pentaplacodinium lapazense PEJV-4a OP806525
100/-
100/-
100/-
100/0.93
100/-
100/0.99
100/0.96
64/-
0.1

Figure 14

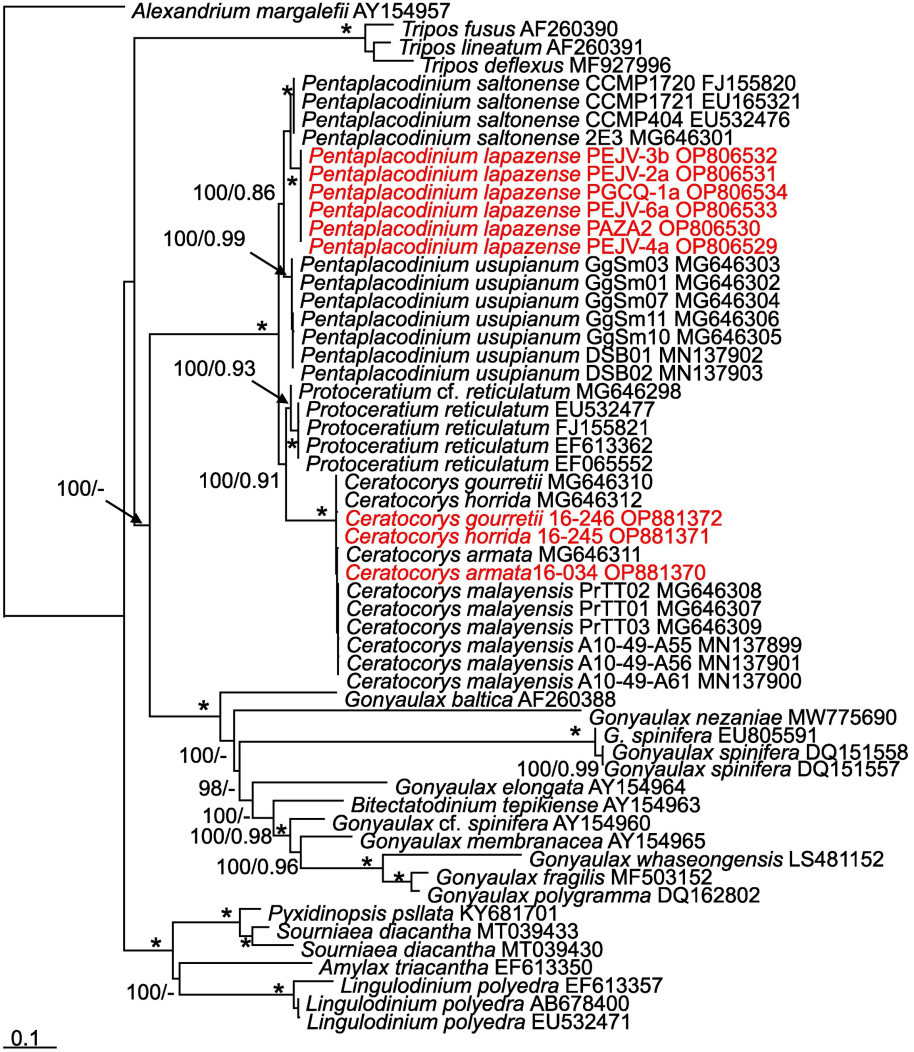
Alexandrium margalefii AY154957
Tripos fusus AF260390
Tripos lineatum AF260391
Tripos deflexus MF927996
Pentaplacodinium saltonense CCMP1720 FJ155820
Pentaplacodinium saltonense CCMP1721 EU165321
Pentaplacodinium saltonense CCMP404 EU532476
Pentaplacodinium saltonense 2E3 MG646301
Pentaplacodinium lapazense PEJV-3b OP806532
Pentaplacodinium lapazense PEJV-2a OP806531
Pentaplacodinium lapazense PGCQ-1a OP806534
Pentaplacodinium lapazense PEJV-6a OP806533
Pentaplacodinium lapazense PAZA2 OP806530
Pentaplacodinium lapazense PEJV-4a OP806529
Pentaplacodinium usupianum GgSm03 MG646303
Pentaplacodinium usupianum GgSm01 MG646302
Pentaplacodinium usupianum GgSm07 MG646304
Pentaplacodinium usupianum GgSm11 MG646306
Pentaplacodinium usupianum GgSm10 MG646305
Pentaplacodinium usupianum DSB01 MN137902
Pentaplacodinium usupianum DSB02 MN137903
Protoceratium cf. reticulatum MG646298
Protoceratium reticulatum EU532477
Protoceratium reticulatum FJ155821
Protoceratium reticulatum EF613362
Protoceratium reticulatum EF065552
Ceratocorys gourretii MG646310
Ceratocorys horrida MG646312
Ceratocorys gourretii 16-246 OP881372
Ceratocorys horrida 16-245 OP881371
Ceratocorys armata MG646311
Ceratocorys armata16-034 OP881370
Ceratocorys malayensis PrTT02 MG646308
Ceratocorys malayensis PrTT01 MG646307
Ceratocorys malayensis PrTT03 MG646309
Ceratocorys malayensis A10-49-A55 MN137899
Ceratocorys malayensis A10-49-A56 MN137901
Ceratocorys malayensis A10-49-A61 MN137900
Gonyaulax baltica AF260388
Gonyaulax nezaniae MW775690
G. spinifera EU805591
Gonyaulax spinifera DQ151558
Gonyaulax spinifera DQ151557
Gonyaulax elongata AY154964
Bitectatodinium tepikiense AY154963
Gonyaulax cf. spinifera AY154960
Gonyaulax membranacea AY154965
Gonyaulax whaseongensis LS481152
Gonyaulax fragilis MF503152
Gonyaulax polygramma DQ162802
Pyxidinopsis psllata KY681701
Sourniaea diacantha MT039433
Sourniaea diacantha MT039430
Amylax triacantha EF613350
Lingulodinium polyedra EF613357
Lingulodinium polyedra AB678400
Lingulodinium polyedra EU532471
100/0.86
100/0.99
100/0.93
100/0.91
100/-
100/-
98/-
100/-
100/0.98
100/0.96
100/-
0.1

Figure 15

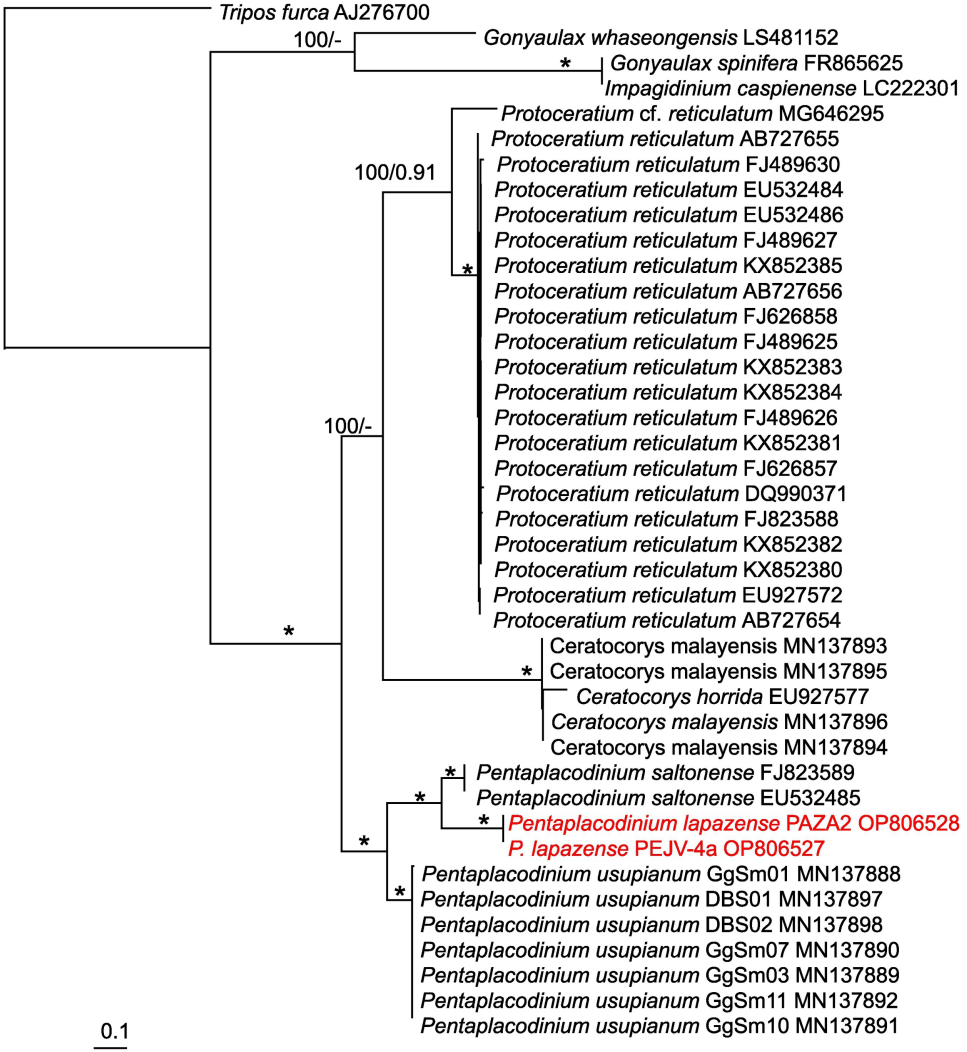
Tripos furca AJ276700
100/-
Gonyaulax whaseongensis LS481152
*
Gonyaulax spinifera FR865625
Impagidinium caspienense LC222301
Protoceratium cf. reticulatum MG646295
Protoceratium reticulatum AB727655
100/0.91
Protoceratium reticulatum FJ489630
Protoceratium reticulatum EU532484
Protoceratium reticulatum EU532486
Protoceratium reticulatum FJ489627
*
Protoceratium reticulatum KX852385
Protoceratium reticulatum AB727656
Protoceratium reticulatum FJ626858
Protoceratium reticulatum FJ489625
Protoceratium reticulatum KX852383
Protoceratium reticulatum KX852384
100/-
Protoceratium reticulatum FJ489626
Protoceratium reticulatum KX852381
Protoceratium reticulatum FJ626857
Protoceratium reticulatum DQ990371
Protoceratium reticulatum FJ823588
Protoceratium reticulatum KX852382
Protoceratium reticulatum KX852380
Protoceratium reticulatum EU927572
Protoceratium reticulatum AB727654
*
Ceratocorys malayensis MN137893
*
Ceratocorys malayensis MN137895
Ceratocorys horrida EU927577
Ceratocorys malayensis MN137896
Ceratocorys malayensis MN137894
*
Pentaplacodinium saltonense FJ823589
*
Pentaplacodinium saltonense EU532485
*
Pentaplacodinium lapazense PAZA2 OP806528
*
P. lapazense PEJV-4a OP806527
*
Pentaplacodinium usupianum GgSm01 MN137888
*
Pentaplacodinium usupianum DBS01 MN137897
Pentaplacodinium usupianum DBS02 MN137898
Pentaplacodinium usupianum GgSm07 MN137890
Pentaplacodinium usupianum GgSm03 MN137889
Pentaplacodinium usupianum GgSm11 MN137892
Pentaplacodinium usupianum GgSm10 MN137891
0.1

Figure 16

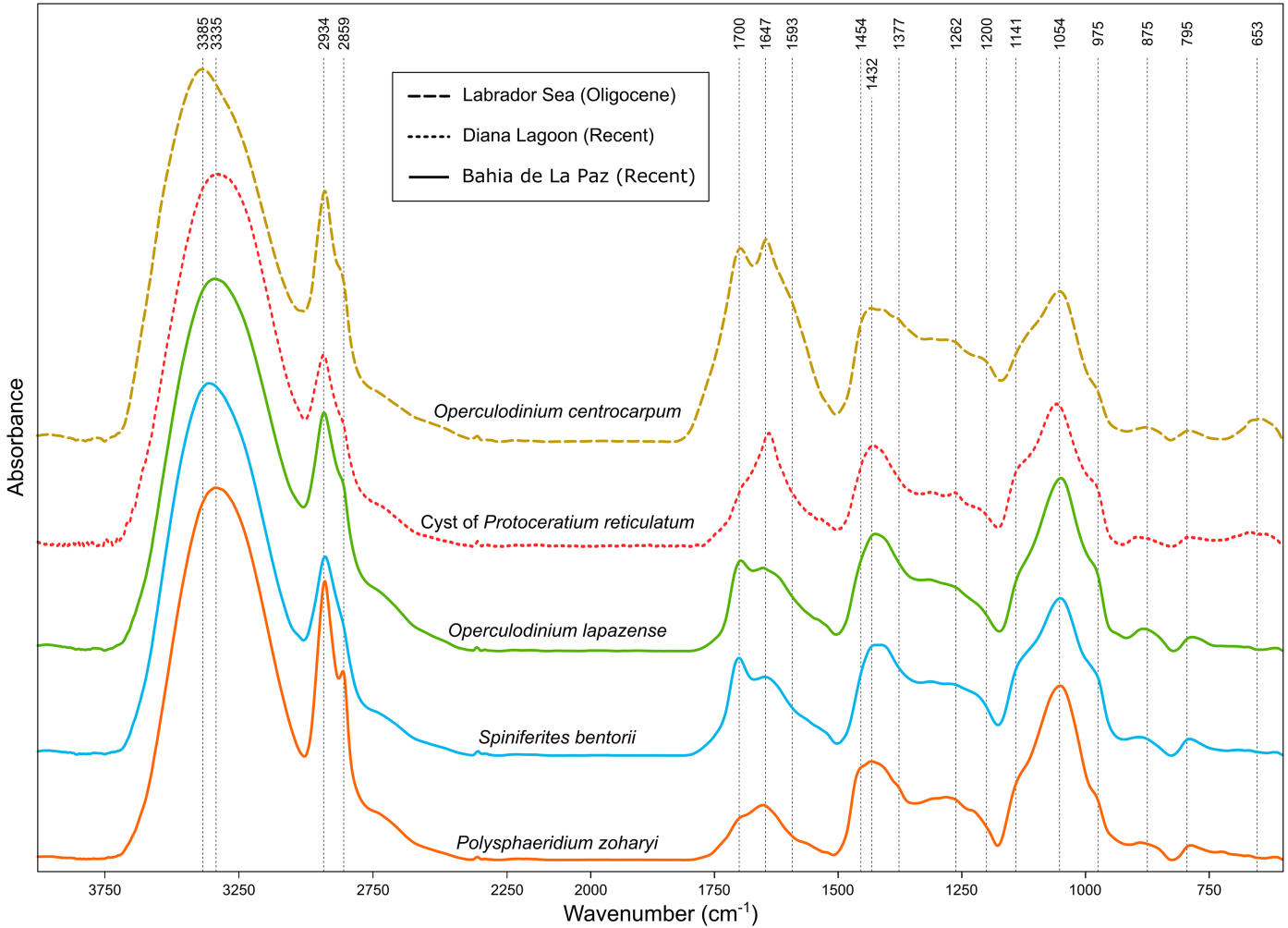
3385
3335
2934
2859
1700
1647
1593
1454
1432
1377
1262
1200
1141
1054
975
875
795
653
Labrador Sea (Oligocene)
Diana Lagoon (Recent)
Bahia de La Paz (Recent)
Operculodinium centrocarpum
Cyst of Protoceratium reticulatum
Operculodinium lapazense
Spiniferites bentorii
Polysphaeridium zoharyi
Absorbance
3750
3250
2750
2250
2000
1750
1500
1250
1000
750
Wavenumber (cm-1)

Figure 17